12 Seismic Anisotropy and Global Geodynamics

Jean-Paul Montagner[1,2,3] **and Laurent Guillot**[1]

[1] *Seismological Laboratory, CNRS URA 195*
Institut de Physique du Globe, Paris, France

[2] On leave at: *Seismological Laboratory*
California Institute of Technology, 252-21
Pasadena, California 91125

[3] On leave at: *Jet Propulsion Laboratory*
California Institute of Technology
4800 Oak Grove Drive, Pasadena, California 91109

INTRODUCTION

For many years, seismic anisotropy was often neglected, mostly because of the inherent heavy mathematical and computational tools needed to describe and model its effects on seismic waves. The usual basic knowledge about propagation in isotropic media cannot easily apply to anisotropic media, where new phenomena come up, such as birefringence (or shear-wave splitting), or difference between directions of propagation of phase velocity and of group velocity. Consequently, geophysicists often claimed that it was a second-order effect, and considered the Earth as isotropic.

This hypothesis was assumed to be a good approximation, because of the random orientation of crystals in most parts of the Earth, and of the random sampling of anisotropic regions by seismic rays. This assumption furthermore made easier the description of wave propagation, as well as the parameterization of media in inverse problems. An isotropic elastic medium can be described by two independent elastic parameters (λ and μ Lamé parameters), but the simplest anisotropic medium (transverse isotropy with a vertical symmetry axis) requires 5 independent parameters (Love 1927, Anderson 1961). To date, seismic observations have been explained in terms of isotropic (and often thermal) lateral heterogeneities, ignoring manifestations of anisotropy. However, since the 1960s, it was recognized that most parts of the Earth are not only laterally heterogeneous but also anisotropic and that seismic anisotropy provides a simple explanation of different observational data:

- azimuthal variation of Pn-velocities below oceans (discovered in the 1960s; Hess (1964) explained it by anisotropy),
- Rayleigh-Love wave discrepancy: It is impossible to simultaneously explain Rayleigh and Love wave dispersion by an isotropic model (Anderson 1961, Aki and Kaminuma 1963, Mc Evilly 1964),
- Shear-wave splitting (or birefringence), the most unambiguous observation of anisotropy, particularly for SKS waves (Vinnik et al. 1984).

Seismic anisotropy, contrary to isotropy, is reflecting some inherent *organization* of the matter. Different geophysical fields are involved in the investigation of the manifestations of anisotropy of Earth materials: mineral physics and geology for the study of the microscopic scale, seismology and geodynamics for scales larger than typically one kilometer. The origin of seismic anisotropy is non-unique. In the crust, the crack distribution seems to play a major role (Crampin and Booth 1985). In the upper mantle, it is usually explained by the lattice-preferred orientation of α-olivine (Nicolas and Christensen 1987, Zhang and Karato 1995) and is related to plate-tectonic processes. More generally the intrinsic anisotropy of minerals (olivine and to a less extent orthopyroxene and clinopyroxene) associated with their lattice-preferred orientation may induce large-

1529-6466/00/0051-0012$05.00

scale observable and unambiguous effects, either on body waves (S-wave splitting observed on SKS (Vinnik et al. 1984), P-wave anisotropy (Babuska et al. 1984) or surface waves through the azimuthal anisotropy (Forsyth 1975) and the radial (improperly named "polarization") anisotropy (Schlue and Knopoff 1977). These different measurements of anisotropy performed at different spatial scales were difficult to reconcile.

Investigating deeper lower mantle anisotropy is a formidable challenge, because the anisotropy signal is small, often masked by upper mantle anisotropy, and its physical explanation is controversial. Most of the lower mantle seems to be isotropic (Meade et al. 1995), except the D″-layer (Vinnik et al. 1989b, Maupin 1994) where anisotropy could result from the layering of old subducted slabs and/or melted materials. Even deeper, anisotropy has also been found in the inner core from free oscillations (Woodhouse et al. 1986) and from the P-wave travel times reported in the ISC bulletins (Morelli et al 1986). The origin, amplitude and mechanisms creating the anisotropy in the core are still subject of controversy (e.g., see Singh et al. 2000). Since these early observations of seismic anisotropy, a large and rapidly growing number of studies have confirmed its existence in the different depth ranges of the Earth. A complete and exhaustive review of these studies is beyond the scope of this paper, and, we will only underline their geodynamic implications.

From the global geodynamics point of view, seismic anisotropy has many applications, although it is still in its infancy. We will show how it makes it possible to define the root of continents and to investigate the coupling between the lithosphere and the rest of the mantle (Montagner and Tanimoto 1991, Silver 1996), and more generally to gain insight into mantle convection (Anderson and Regan 1984, Montagner 1994). Mantle convection characterized by a high Rayleigh number is highly chaotic and numerical modeling demonstrates that most of the deformation takes place in boundary layers. Conversely, since seismic anisotropy is closely related to large-scale deformation (Nicolas and Christensen 1987, Karato 1989), boundary layers can be detected by the existence of seismic anisotropy (Montagner 1998, Karato 1998).

We present in this paper the different depth ranges in the mantle, where seismic anisotropy was detected, i.e., uppermost mantle, transition zone and D″-layer. In the top boundary layer of the mantle, seismic anisotropy can be directly compared to geological observations. The robust features of these different investigations in different depth ranges are presented and the enormous scientific potential of seismic anisotropy is emphasized.

CAUSES OF SEISMIC ANISOTROPY FROM MICROSCOPIC TO LARGE SCALE

Many processes can give rise to seismic anisotropy, and we must be very careful when interpreting it. They can be related either to anisotropic structural settings in rocks, or to the intrinsic anisotropy of minerals in the Earth.

Shape Preferred Orientation (S.P.O.)

Anisotropic spatial organization of matter (even though isotropic) can induce seismic anisotropy:

- a fine layering of heterogeneous rocks (even though isotropic) is "seen" as transversely isotropic by a wave whose wavelength is larger than the typical thickness of layers (Backus 1962). Some authors proposed that this kind of structure, observed in ophiolites for instance, could result from the progressive mixing of rocks with heterogeneous mechanical properties and could explain the seismic anisotropy in the Earth's upper mantle (e.g., the "marble cake" of Allègre and Turcotte 1986);
- distribution of cracks (Crampin and Booth 1985) and/or fluid inclusions can induce

anisotropy (probably an important effect in the crust and in the inner core).

Lattice Preferred Orientation (L.P.O.)

Some major mineral phases of the Earth's mantle are anisotropic in elasticity. Under some conditions, plastic deformation of these minerals can result in a preferential orientation of their lattices. This phenomenon is often considered as the origin of the large-scale seismic anisotropy in the upper mantle. We present below in a very simplified manner the conditions required to develop such a seismic anisotropy. A complete discussion of these different mechanisms at different scales can be found in recent extensive and well-documented review papers (Kendall 2000, Mainprice et al. 2000, Savage 1999).

Intrinsic anisotropy of minerals. Some minerals present in the upper mantle are strongly anisotropic (see Mainprice et al. 2000 and references therein for an exhaustive review of the minerals and their anisotropic properties). The difference of P-wave velocity between the fast axis and the slow axis is larger than 20% for olivine, the main constituent of the upper mantle. Other important constituents such as orthopyroxene or clinopyroxene are anisotropic as well (>10%) (see Anderson 1989, or Babuska and Cara 1991). Some other constituents such as garnet display a very small intrinsic anisotropy. With increasing the depth, most of minerals undergo a series of phase transformations. There is some tendency (though not systematic), that with increasing pressure (whose effect is predominant in the mantle), the crystallographic structure evolves towards a more closely packed, more isotropic structure, such as cubic structure. For example, olivine transforms into β-spinel and then γ-spinel in the upper transition zone (410 to 660 km depth) and into perovskite and magnesiowüstite in the lower mantle; but perovskite $(Mg,Fe)SiO_3$ and the pure end-member of magnesiowüstite MgO are still anisotropic. That could explain the observed anisotropy in some parts of the lower mantle (Karato 1998, or MacNamara et al. 2002).

Efficient mechanisms of orientation of crystals. In order to observe seismic anisotropy, the crystals must be sensitive to the strain field, and a lattice preferred orientation must develop either from dislocation creep (activation of slip systems) or from dynamic recrystallization (see Karato (1989) and Poirier (1985), for a phenomenological description, and Ribe (1989) and Kaminski and Ribe (2001), e.g., for numerical modeling). Through the mechanisms of lattice-preferred orientation, it is found that the anisotropy of an aggregate of many minerals can be very large (Nicolas and Christensen 1987). In the lower mantle super-plasticity may be the predominant deformation mechanism, and that may cause the absence of large scale seismic anisotropy in this part of the Earth (Karato 1998).

Anisotropy of assemblages of minerals. Mantle rocks are assemblages of different minerals which are more or less anisotropic. The amount of anisotropy is largely dependent on the composition of the aggregates. The relative orientations of crystallographic axes in the different minerals must not counteract in destroying the intrinsic anisotropy of each mineral. For example, the anisotropy of peridotites, mainly composed of olivine and orthopyroxene, is affected by the relative orientation of their crystallographic axes (Christensen and Lundquist 1982). According to their observations, the fast axis of olivine is parallel to the intermediate axis of orthopyroxene in the shear plane and parallel to the flow direction, but the fast axis of orthopyroxene and the slow axis of olivine are orthogonal to the shear plane (Fig. 1). The resulting anisotropy for P-waves, however, is larger than 10% (Peselnick and Nicolas 1978). Such a large anisotropy is consistent on intermediate scale, for instance in massifs of ophiolites, which present such an anisotropy over several tens of kilometers (Nicolas 1993, Vauchez and Nicolas 1991).

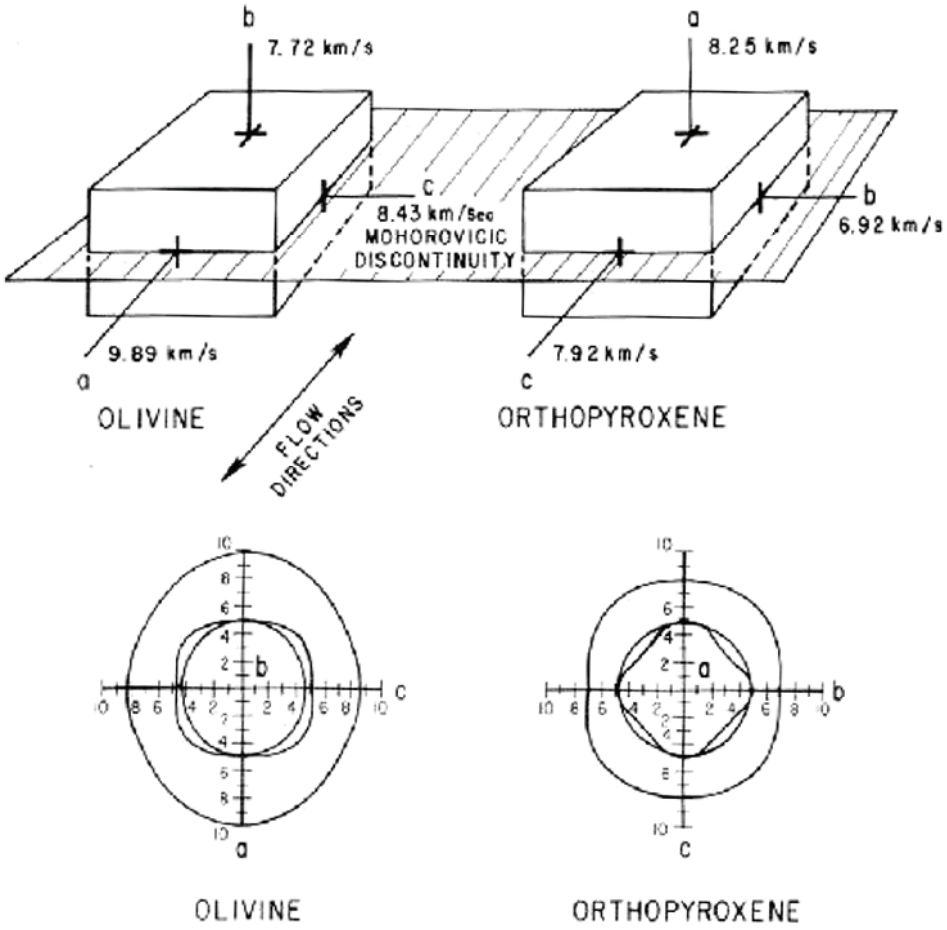

Figure 1. Figure of Christensen and Lundquist (see Anderson 1989) for olivine and orthopyroxene orientation). This observation is the base of the interpretation of seismic anisotropy in terms of convective flow.

Coherent strain field. At large scale, the deformation due to mantle convection must be coherent over large distances in order to preserve long wavelength anisotropy. From Pn studies and models of formation of the oceanic lithosphere, it is possible to infer that anisotropy remains uniform on horizontal length-scales in excess of 1000 km.

Under those assumptions it is possible to estimate the effect of LPO-induced anisotropy on body-wave speeds, and compare it with thermal effects (Montagner and Guillot 2000). The magnitude of seismic anisotropy can be estimated in a simplified geodynamical context such as an oceanic convective cell, for a simplified mineralogical composition (60% olivine, 40% orthopyroxene). The relative orientation of the crystalline populations in the kinematic field is that discussed in the previous section, and we neglect the dispersion of the orientations around this perfect or ideal orientation. The general method followed for the calculation of anisotropic parameters is summarized in Figure 2. Body-wave velocities are calculated along 4 vertical profiles, from the surface down to the 410-km-discontinuity (Fig. 3): at the mid-ocean ridge and along a slab, which are characteristic of hot or cold vertical currents; for a 7-Myr-old lithosphere and for a 30-Myr-old lithosphere from the ridge, where horizontal currents are dominant. Some other profiles are reported in Montagner and Guillot (2000) for a pure olivine upper mantle. The amplitude of the temperature effect (ΔT) can be roughly estimated by comparing the ridge and the slab profiles displaying the same orientations of minerals. It is found around 3 to 4%. The differences in *PH*-waves velocities (horizontally-polarized P-waves) between

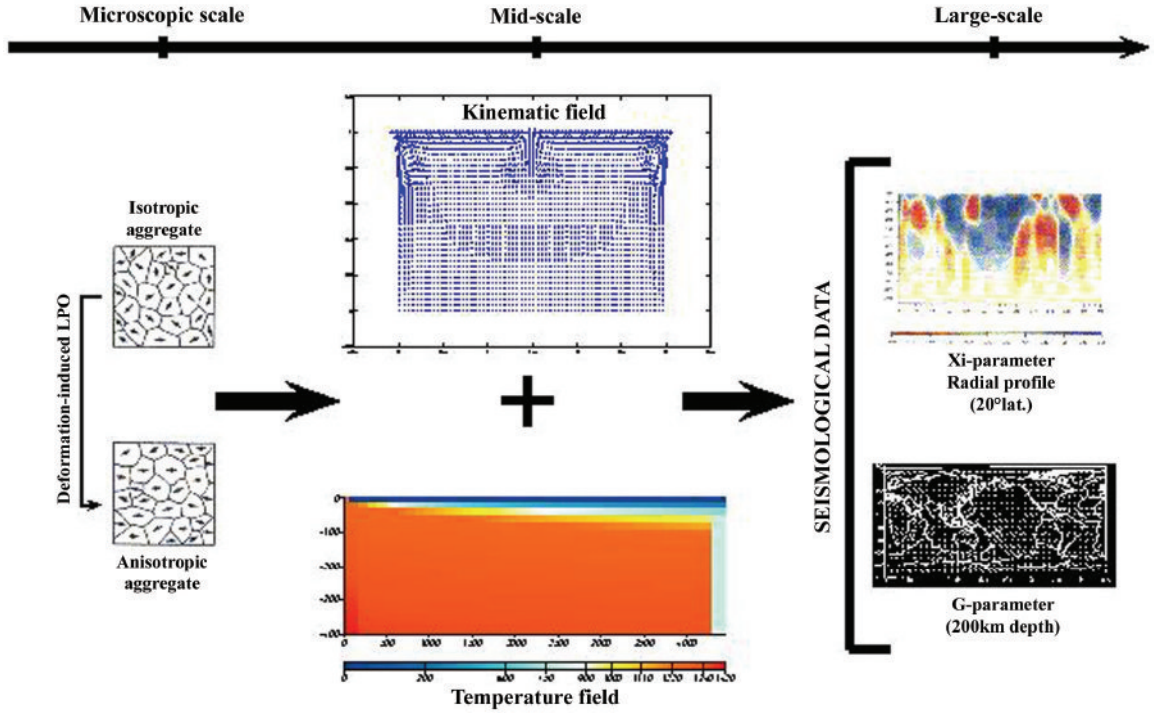

Figure 2. Different steps from mineralogical anisotropy at microscopic scale to observable seismic anisotropy at large scale.

vertical and horizontal currents are mostly due to the orientation of crystals (effect symbolized by $\Delta\alpha$ on Fig. 3). When comparing these velocities with those obtained for an equivalent isotropic system (Voigt average, see Appendix B), the magnitude of anisotropic effects on *PH*-wave (resp. *SV*-wave) velocities (Fig. 3) is about ±3%, which is slightly higher than thermal effects in vertical currents (except at the ridge). Even though anisotropy in the upper mantle should be weaker than in those experiments (natural dispersion of the crystallites), its effect on seismic properties might be as high as thermal effects; that underlines the importance of including anisotropic effects in tomographic studies.

EFFECT OF ANISOTROPY ON SEISMIC WAVES

The effect of seismic anisotropy on seismic waves has been extensively investigated since Love (1927). The reader is referred to the classical textbooks of Fedorov (1968) and Helbig (1994) and their application to Earth sciences (Anderson 1989, Babuska and Cara 1991). The basic theory of seismic wave propagation in anisotropic media is briefly presented in the Appendix A. The complexity of the effect of elastic anisotropy results from the general linear relationship between the stress tensor components σ_{ij} and the strain tensor components ε_{kl} which involve a fourth-order elastic tensor C_{ijkl} This relationship is named the generalized Hooke's law:

$$\sigma_{ij} = C_{ijkl}\, \varepsilon_{kl} \tag{1}$$

The elastic tensor, C, in the most general case, presents 21 independent parameters. How to deal with this tensor is briefly described in the Appendix B. There are two ways to manage such complexity of C: (1) by considering either that the medium possesses symmetry properties (in order to decrease the number of independent elastic moduli) and

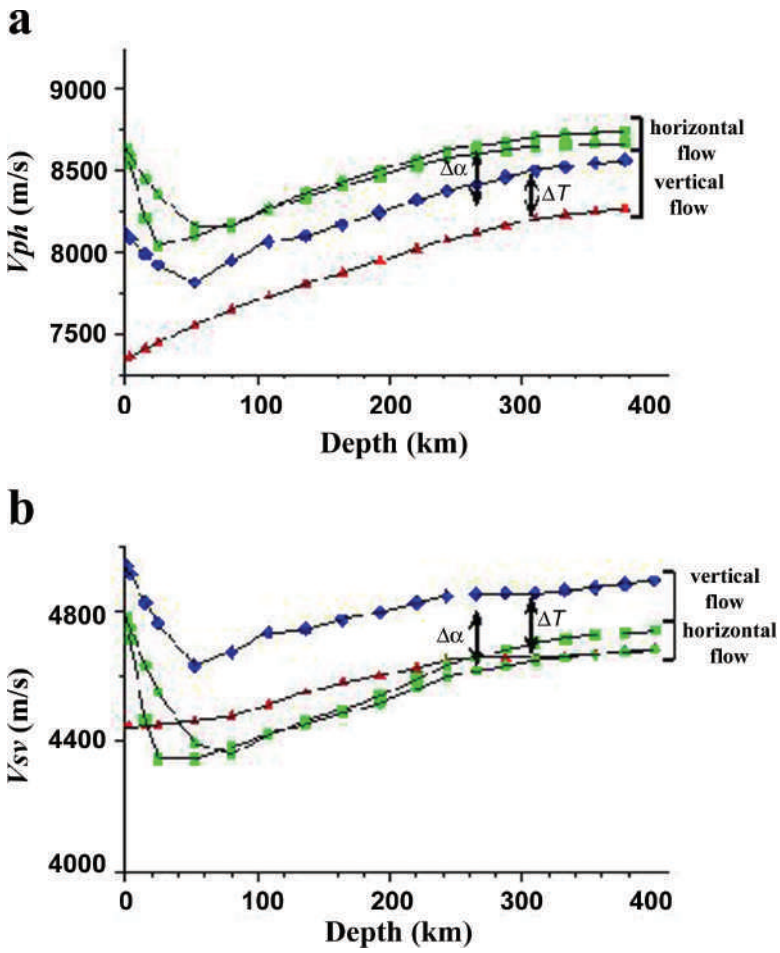

Figure 3. V_{PH} and V_{SV} velocity profiles for a 60-40 olivine-orthopyroxene upper mantle within the convecting cell displayed in Figure 1 (from Montagner and Guillot 2000). Diamond: slab; Δ : ridge; □ : 7-Myr-old plate; ❍ : 30-Myr-old plate. The arrows represent rough approximations of the effects of orientation (Δα) and temperature (Δ*T*) on body wave velocities.

ultimately that it is isotropic, (2) or that the seismic anisotropy is a first-order perturbation, which permits the application of classical perturbation theories (Backus 1965). Except an isotropic medium defined by 2 elastic moduli (λ and μ), the simplest case of anisotropic medium is the transversely isotropic (TI) medium (hexagonal symmetry), characterized by 5 independent parameters A, C, F, L, N (Love 1927) when the symmetry axis is vertical. This parameterization with a vertical symmetry axis was used in deriving PREM (preliminary reference Earth model) by Dziewonski and Anderson (1981). It corresponds to the most general case for a spherically symmetric model. A slightly more complex parameterization is the TI case with a tilted symmetry axis (hexagonal symmetry), which adds 2 additional angular parameters defining the orientation of the axis. The perturbation theory is well suited for investigating the anisotropic structure of the deep Earth. As demonstrated in the first section, seismic anisotropy is not a second-order effect but, due to several averaging processes, it is usually smaller than 10%, enabling the application of perturbation theories. Seismologists are working in this framework for body waves, surface waves and normal modes.

Body waves

From a theoretical point of view, a first application of perturbation theory to body waves was performed by Backus (1965) and then extensively applied (Crampin 1984, for a first review paper). In the case of a weak anisotropy, we can consider that the

polarization of the three solutions of the Christoffel equation (see Appendix A) is very close to P, SH and SV waves. Let us call V_P, V_{S1} and V_{S2} the velocities of quasi-P, quasi-SV and quasi-SH waves. We draw the attention that since the sagittal plane (plane defined by the ray trajectory) is not necessarily a symmetry plane, the SV and SH components of the incoming wave may be different from the S_1 and S_2 components of quasi SH and SV waves. For a wave propagating horizontally in the plane (1,2) with azimuth Ψ and where 3- is the vertical direction, the different velocities are given by the following expressions in the symmetry planes:

$$\rho V_P^2 = 1/8\,(C_{1111}+2(C_{1122}+C_{1212})+3C_{2222}) + 1/2\,(C_{1111}-C_{2222})\cos2\psi + (C_{2111}+C_{1222})\sin2\psi + 1/8\,(C_{1111}-2(C_{1122}+C_{1212})+C_{2222})\cos4\psi + 1/2\,(C_{2111}-C_{1222})\sin4\psi \quad (2a)$$

$$\rho V_{S1}^2 = 1/8\,(C_{1313}+C_{2323}) + 1/2\,(C_{1313}-C_{2323})\cos2\psi + C_{2313}\sin2\psi \quad (2b)$$

$$\rho V_{S2}^2 = 1/8\,(C_{1111}-2(C_{1122}-C_{1212})+C_{2222}) - 1/8\,(C_{1111}-2(C_{1122}+C_{1212})+C_{2222})\cos4\psi - 1/2\,(C_{2111}-C_{1222})\sin4\psi \quad (2c)$$

These expressions are not general, but are extensively used when assuming a TI medium with any symmetry axis. This case is a very good approximation for the upper mantle pyrolitic model (Estey and Douglas 1986).

For body waves, the evidence of anisotropy primarily results from the investigation of the splitting in teleseismic shear waves (Fig. 4a) such as SKS (Vinnik et al. 1984, 1989a,b, 1991, 1992; Silver and Chan 1988, 1991; Ansel and Nataf 1989), ScS (Ando 1984, Fukao 1984) and S (Ando et al. 1983; Bowman and Ando 1987; Fischer et al. 1996; Gaherty and Jordan 1995), which is corroborated by the evidence of P-wave anisotropy (Babuska et al. 1984, 1993). Among these different observations, the splitting information derived from SKS is probably the less ambiguous and has been extensively used in teleseismic anisotropy investigations. See Silver (1996) and Kendall (2000) for reviews. The drawbacks of SKS observations are, that it is almost impossible to precisely locate the depth of anisotropic regions, nor to take account for a dipping symmetry axis, and that only continental areas can be extensively investigated. The rapid variation of directions of fast velocity which can be observed in some continental regions on a short spatial scale (Vinnik et al. 1989a, Hirn et al. 1995), cannot be explained by a very deep anisotropy and the origin of anisotropy is confined to the first 410 km, either in the lithosphere or in the top of the asthenosphere. However, there are some first attempts to introduce more complex radial models of anisotropy. A close examination of SKS data makes it necessary, in several areas, to introduce at least two layers of anisotropy with different amplitudes and directions (Silver and Savage 1994, Farra and Vinnik 1994, Girardin and Farra 1998, Savage 1998, Wolfe and Silver 1998). A map summarizing the different observations of SKS splitting is presented in Figure 4b, which is an upgrade by Savage (1999) of the compilation of Silver (1996).

Surface waves

Surface waves are also well suited for investigating upper mantle anisotropy. Contrary to body waves, surface waves enable us to locate anisotropy at depth but, so far, its lateral resolution (several thousands of kilometers) is very poor. Two kinds of observable anisotropy have been considered. The first one results from the well-known discrepancy between Love and Rayleigh waves (Anderson 1961, McEvilly 1964), often referred as the "polarization" anisotropy (Schlue and Knopoff 1977) or the radial anisotropy. In order to remove this discrepancy, it is sufficient to consider a TI medium with a vertical symmetry axis, characterized by five elastic parameters plus density. On a global scale, Nataf et al. (1984, 1986), by the simultaneous inversion of Rayleigh and Love wave dispersion, derived the geographical distributions of S-wave radial anisotropy

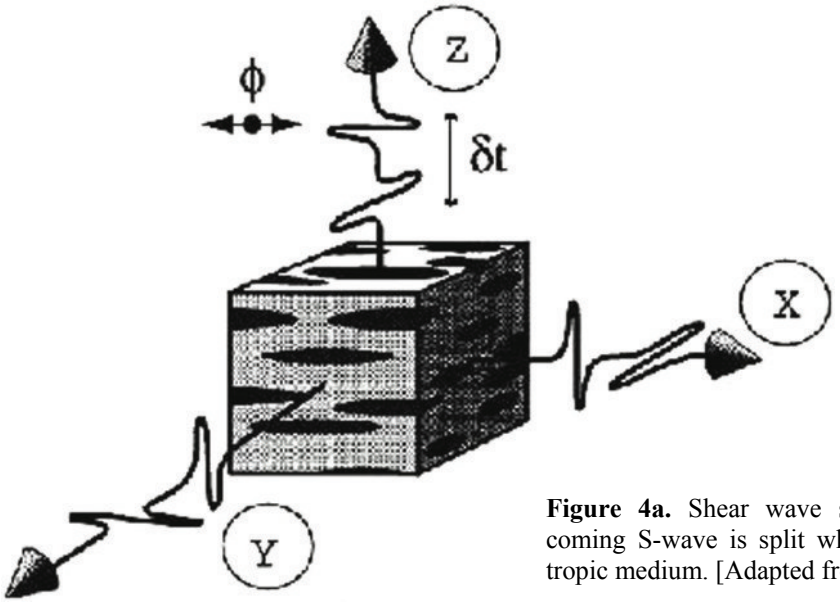

Figure 4a. Shear wave splitting. How an incoming S-wave is split when crossing an anisotropic medium. [Adapted from Silver (1996).]

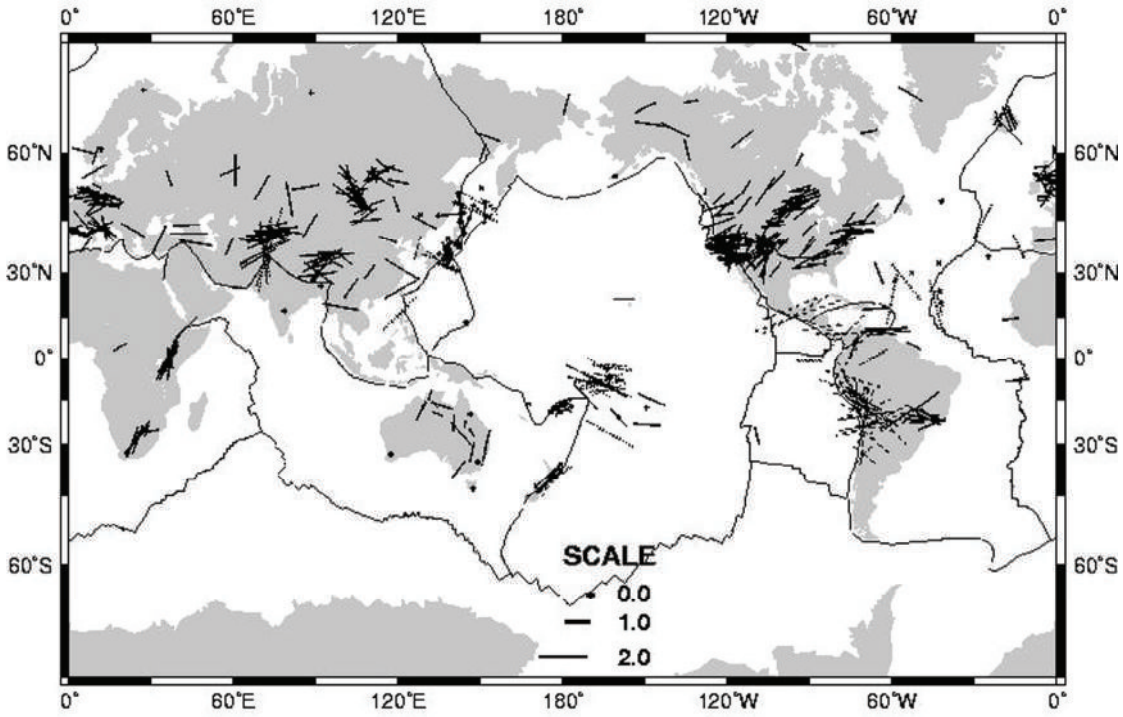

Figure 4b. Shear wave splitting. Compilation of worldwide shear wave splitting measurements. [Adapted from Savage (1999).]. This dataset includes primarily SKS data but also S, ScS, SS, and PS data.

at different depths. Lévêque and Cara (1985), Cara and Lévêque (1988) used higher mode data to display radial anisotropy under the Pacific Ocean and North America down to at least 300 km. The second kind of observable anisotropy is the azimuthal anisotropy, directly derived from the azimuthal variation of phase velocity of surface waves. It was observed for the first time on Rayleigh waves by Forsyth (1975) in Nazca plate. Since these pioneering studies, global and regional models have been derived for both kinds of anisotropy (Mitchell and Yu 1980, Montagner 1985). Tanimoto and Anderson (1985) obtained a global distribution of the Rayleigh wave azimuthal anisotropy at different

periods. On a regional scale, several tomographic investigations reported in the eighties the existence of azimuthal anisotropy in the Indian Ocean (Montagner 1986a), Pacific Ocean (Suetsugu and Nakanishi 1987, Nishimura and Forsyth 1989) and in Africa (Hadiouche et al. 1989).

The radial anisotropy (or "polarization" anisotropy) and the azimuthal anisotropy are two different manifestations of a same phenomenon, the anisotropy of the upper mantle. Montagner and Nataf (1986) derived a technique that makes it possible to simultaneously explain these two forms of seismically observable anisotropy. The principles of this technique will be only briefly described, for the most general case of anisotropy (provided that it is small). A complete description of the whole procedure can be found in Montagner (1996, 1998). Most of these measurements are based on the phase of waves. But it is now possible to use amplitude data by looking at polarization anomalies (Yu and Park 1994, Larson et al. 1998, Laske and Masters 1998, Pettersen and Maupin 2002).

From a theoretical point of view, a general slight elastic anisotropy in a plane-layered medium gives rise to an azimuthal dependence of the local phase or group velocities of Love and Rayleigh waves at point (θ,ϕ) along the ray of the form (Smith and Dahlen 1973, 1975):

$$V(\omega,\theta,\phi,\Psi) - V_0(\omega,\Psi) = \alpha_0(\omega,\theta,\phi) + \alpha_1(\omega,\theta,\phi)\cos 2\Psi + \alpha_2(\omega,\theta,\phi)\sin 2\Psi + \alpha_3(\omega,\theta,\phi)\cos 4\Psi + \alpha_4(\omega,\theta,\phi)\sin 4\psi \quad (3)$$

where ω is the frequency of the wave, $V_0(\omega,\Psi)$ the reference velocity of the unperturbed medium, and Ψ is the azimuth along the path. The local phase velocity $V(\omega,\theta,\phi,\Psi)$ is used to calculate the travel time between the epicenter E and the receiver R, which is easily related to the measurement of the along-path averaged phase velocity $V_d(\omega)$:

$$t_{E\to R} = \Delta/V_d(\omega) = \int_E^R \frac{ds}{V(\omega,\theta,\phi,\Psi)} \quad (4)$$

Montagner and Nataf (1986), following the same approach as Smith and Dahlen (1973), displayed that simple linear combinations of the elastic tensor components C_{ij} are sufficient to describe the two seismically observable effects of anisotropy on surface waves. For the Voigt notation of the elastic constants (two indices instead of four), see Appendix B. The 0-Ψ term corresponds to the average over all azimuths and involves 5 independent parameters, A, C, F, L, N, which express the equivalent transversely isotropic medium with vertical symmetry axis. The other azimuthal terms (2-Ψ and 4-Ψ) depend on 4 groups of 2 parameters, B, G, H, respectively describing the 2-Ψ azimuthal variation of A, L, F, and E describing the 4-Ψ azimuthal variation of A and N. Therefore, the different azimuthal terms α_0, α_1, α_2, α_3, α_4, depend on 13 3-dimensional parameters, which are assumed independent:

- Constant term (0-Ψ azimuthal term: α_0)

$$\begin{aligned} A &= \rho V_{PH}^2 = 3/8(C_{11}+C_{22}) + 1/4C_{12} + 1/2C_{66} \\ C &= \rho V_{PV}^2 = C_{33} \\ F &= 1/2(C_{13}+C_{23}) \\ L &= \rho V_{SV}^2 = 1/2(C_{44}+C_{55}) \\ N &= \rho V_{SH}^2 = 1/8(C_{11}+C_{22}) - 1/4C_{12} + 1/2C_{66} \end{aligned} \quad (5a)$$

- 2-Ψ azimuthal term:

$$\begin{aligned} B_C &= 1/2(C_{11}-C_{22}) \\ G_C &= 1/2(C_{55}-C_{44}) \\ H_C &= 1/2(C_{13}-C_{23}) \end{aligned}$$

$$B_S = C_{16} + C_{26}$$
$$G_S = C_{54} \quad (5b)$$
$$H_S = C_{36}$$

- 4-Ψ azimuthal term:

$$E_C = 1/8(C_{11}+C_{22}) - 1/4C_{12} - 1/2C_{66} \quad (5c)$$
$$E_S = 1/2(C_{16}-C_{26}) \ ,$$

where indices 1 and 2 refer to horizontal coordinates (1: North; 2: East) and index 3 refers to vertical coordinate. ρ is the density, V_{PH}, V_{PV} are respectively horizontal and vertical *propagating* P-wave velocities, V_{SH}, V_{SV} horizontal and vertical *polarized* S-wave velocities. So, the different parameters present in the different azimuthal terms are simply related to elastic moduli C_{ij}. The corresponding kernels are detailed and some of their variations at depth are plotted in Montagner and Nataf (1986). The complete description of anisotropic effects on normal modes in the spherical case can be found Mochizuki (1986) and Tanimoto (1986). In the most general case, 13 parameters are necessary to explain surface wave data (Rayleigh and Love waves) for small anisotropy, but only 4 parameters are well resolved (Montagner and Jobert 1988): the azimuthally averaged S-wave velocity V_S, the radial anisotropy expressed through the ξ parameter [$\xi = (V_{SH}/V_{SV})^2$] where V_{SH} (respectively V_{SV}) is the velocity of S-wave propagating horizontally with horizontal transverse polarization (respectively with vertical polarization), and the G (G_C, G_S) parameters expressing the horizontal azimuthal variation of V_{SV}. ξ was introduced in the reference Earth model PREM (Dziewonski and Anderson 1981) down to 220 km in order to explain a large dataset of free oscillation eigenfrequencies and body wave travel times. The other elastic parameters can be derived by using constraints from petrology in order to reduce the parameter space (Montagner and Anderson 1989a). Two extreme petrological models were used to derive the necessary correlations between anisotropic parameters, the pyrolite model (Ringwood 1975) and the piclogite model (Anderson and Bass 1984, 1986; Bass and Anderson 1984). In the depth inversion process, the smallest correlations between parameters of both models were kept and included in the *a priori* correlation matrix on parameters. This approach was followed by Montagner and Anderson (1989b) to derive an average reference earth model, and by Montagner and Tanimoto (1991) for the first global 3-D anisotropic model.

Figure 5 shows what is expected for the observable parameters V_S, ξ, G, ψ_G in the case of a simple convective cell with LPO. In terms of convective flow, radial anisotropy ξ expresses its vertical ($\xi < 1$) or horizontal character ($\xi > 1$), and the azimuthal anisotropy $\boldsymbol{G}$, can be related to the horizontal flow direction. Conversely, the three maps of V_S, ξ , $\boldsymbol{G}$, can be interpreted in terms of convective flow. These three pieces of information are necessary to correctly interpret the data. For example, upwellings or downwellings are both characterized by a weak or negative ξ parameter, but a correlative positive or negative δV_S discriminates between these possibilities. By simultaneously inverting at depth for the different azimuthal terms of Rayleigh and Love waves, it is therefore possible to separate the lateral variations in temperature from those induced by the orientation of minerals. Such an interpretation should however be erroneous in water-rich mantle regions where LPO of minerals such as olivine is no simply related to the strain field (Jung and Karato 2001). Also note that this interpretation of anisotropy in terms of convective flow, using S-waves speeds only, could be erroneous in a olivine-poor mantle; see Mainprice et al. (2000), e.g., for the relations between lattice preferred orientations and V_P and V_S in the whole orientation space.

The complete tomographic technique (regionalization + inversion at depth) has been applied for investigating either regional structures of the Indian Ocean (Montagner and

Jobert 1988, Debayle and Lévêque 1997), of the Atlantic Ocean (Mocquet et al. 1989, Silveira et al. 1998), of Africa (Hadiouche et al. 1989, Debayle et al. 2001), of Pacific Ocean (Nishimura and Forsyth 1989, Bussy et al. 1993), of Antarctica (Roult et al. 1994), Australia (Debayle and Kennett 2000, Simmons et al. 2002) and Central Asia (Griot et al. 1998a,b) or global structure (Montagner and Tanimoto 1990, 1991; Montagner 2002).

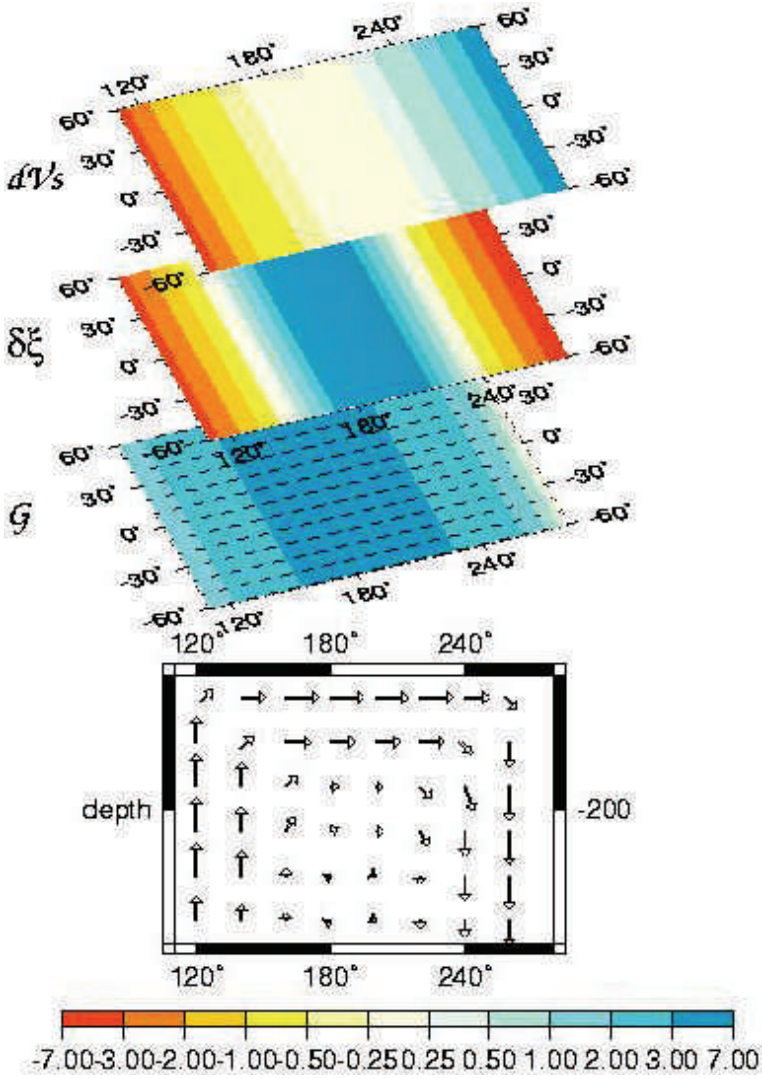

Figure 5. The seismic observable parameters V_S, ξ, G,ψ_G associated with a simple convecting cell in the upper mantle, assuming lattice-preferred orientation of anisotropic minerals such as olivine. A vertical flow is characterized by a negative ξ radial anisotropy (ratio between V_{SH} and V_{SV}) and a small azimuthal anisotropy ($G \approx 0$). An upwelling (resp. downwelling) is characterized by a large positive (resp. negative) temperature anomaly inducing $\delta V_S < 0$ (resp. $\delta V_S > 0$). A predominant large-scale horizontal flow will be translated into a significant amplitude of the G azimuthal anisotropy and its orientation will reflect the direction of flow (with a 180° ambiguity).

Comparison between surface wave anisotropy and SKS splitting data

It can be noted that the anisotropic parameters, linear combinations of elastic moduli C_{ij}, derived from surface waves, also come up when you consider the propagation of body waves in symmetry planes for a slightly anisotropic medium (see section entitled *Body Waves*). A global investigation of anisotropy inferred from SKS body wave splitting measurements (delay times and directions of maximum velocities) has been undertaken by different authors (Vinnik et al. 1992, Silver 1996, Savage 1999). Unfortunately, most

of SKS measurements have been done in continental parts of the Earth, and very few in oceans. It turns out that a direct comparison of body wave and surface wave datasets is now possible (Montagner et al. 2000). If the anisotropic medium is assumed to be characterized by a horizontal symmetry axis with any orientation (that is a very strong assumption), a synthetic dataset of SKS delay times and azimuths can be calculated from the global distribution of anisotropy derived from surface waves, by using the following equation:

$$\delta t_{SKS} = \int_0^h dz \sqrt{\frac{\rho}{L}} \left[\frac{Gc(z)}{L(z)} \cos 2\Psi(z) + \frac{Gs(z)}{L(z)} \sin 2\Psi(z) \right] \tag{6}$$

where δt_{SKS} is the integrated travel time for the depth range *0-h*, where the anisotropic parameters $G_C(z)$,$G_S(z)$ and $L(z)$ are the anisotropic parameters retrieved from surface waves at different depths. It is remarkable to realize that only the *G*-parameter (expressing the SV-wave azimuthal variation) is present in this equation. From Equation (6), we can infer the maximum value of delay time δt_{SKS}^{max} and the corresponding azimuth Ψ_{SKS}:

$$\delta t_{SKS}^{\max} = \sqrt{\left\{ \int_0^h dz \sqrt{\frac{\rho}{L}} \frac{Gc(z)}{L(z)} \right\}^2 + \left\{ \int_0^h dz \sqrt{\frac{\rho}{L}} \frac{Gs(z)}{L(z)} \right\}^2} \tag{7}$$

$$\tan 2\Psi_{SKS} = \frac{\int_0^h dz \sqrt{\frac{\rho}{L}} \frac{Gs(z)}{L(z)}}{\int_0^h dz \sqrt{\frac{\rho}{L}} \frac{Gc(z)}{L(z)}} \tag{8}$$

However, Equation (6) is approximate and only valid when the wavelength is much larger than the thickness of layers. It is possible to make more precise calculations by using the technique derived for 2 layers by Silver and Savage (1994) or by using the general expressions given in Rumpker and Silver (1998) and Montagner et al. (2000). With Equations (7) and (8), a synthetic map of the maximum value of delay time δt_{SKS}^{max} can be obtained by using a 3-D anisotropic surface wave model. A detailed comparison between synthetic SKS derived from AUM (Montagner and Tanimoto 1991) and observed SKS (Silver 1996) was presented in Montagner et al. (2000). Figure 6 shows such a map for the Pacific hemisphere, by using a new anisotropic surface wave model (Montagner 2002) derived from the data of Ekström and Dziewonski (1998). First of all, the comparison shows that both datasets are compatible in magnitude but not necessarily in directions. Some contradictions between measurements derived from surface waves and from body waves have been noted. The agreement of directions is correct in tectonically active areas but not in old cratonic zones. The discrepancy in these areas results from the rapid lateral change of directions of anisotropy at a small scale. These changes stem from the complex history of these areas, which have been built by successive collages of continental pieces. It might also result from the hypothesis of horizontal symmetry axis, which was shown to be invalid in many areas (Plomerova et al. 1996). The positive consequence of this discrepancy is that a small scale mapping of anisotropy in such areas might provide clues for understanding the processes of growth of continents and mountain building.

Contrary to surface waves, SKS-waves have a good lateral resolution, and are sensitive to the short wavelength anisotropy just below the stations. But their drawback is that they have a poor vertical resolution. On the other hand, global anisotropy tomography derived from surface waves only provides long wavelength anisotropy (poor lateral resolution) but enables the location of anisotropy at depth.

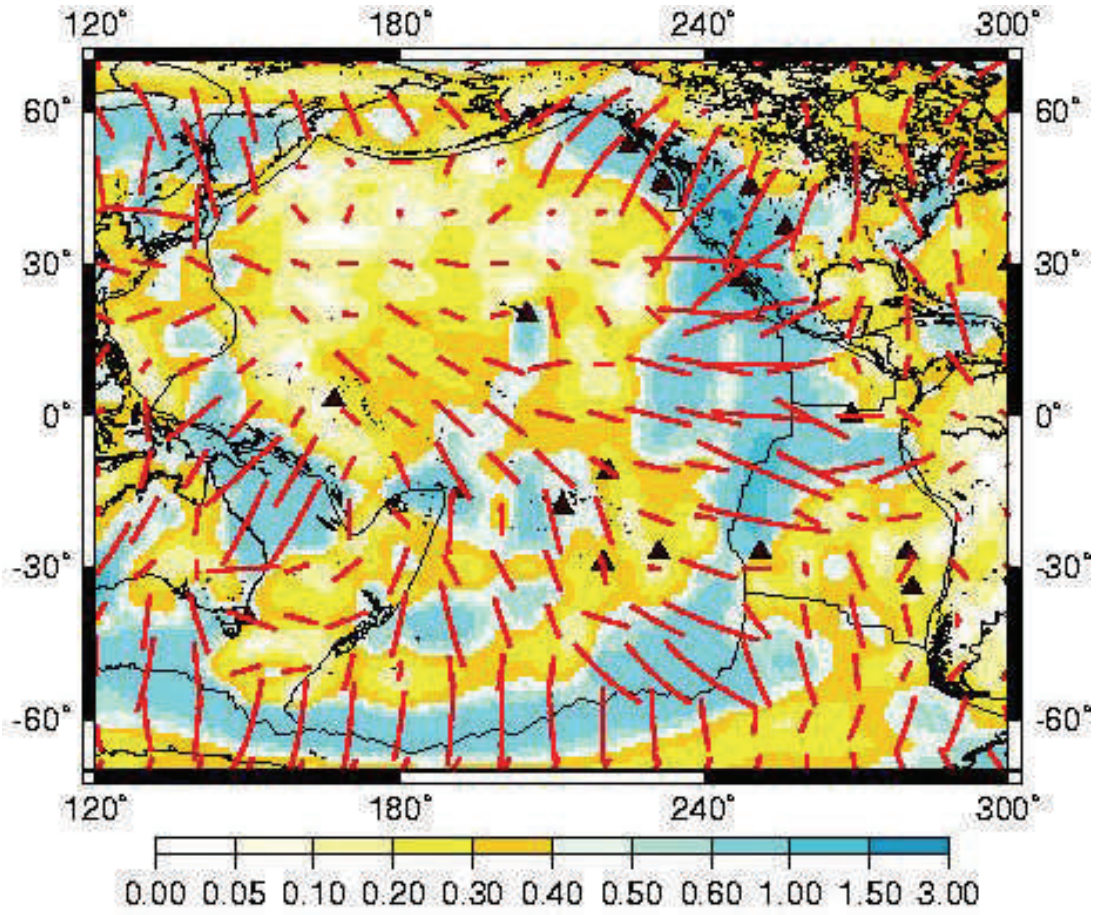

Figure 6. Distributions of synthetic delay time δt_{SKS}^{max} and azimuth Ψ_{SKS} at the surface of the Earth, such as derived from the anisotropic tomographic model of Montagner (2002), derived from data of Ekström and Dziewonski 1998). The crustal part of the 3SMAC -model (Ricard et al. 1996) has been removed. The synthetic map of SKS is calculated by using the method of Montagner et al. (2000), from the G-distribution of V_{SV} azimuthal anisotropy. The length of lines is proportional to δt_{SKS}.

The long wavelength anisotropy derived from surface waves will display the same direction as the short wavelength anisotropy inferred from body waves only when large-scale vertical coherent processes are predominant. As demonstrated by Montagner et al. (2000), the best agreement between observed and synthetic SKS can be found when only layers in the uppermost 200 km of the mantle are taken into account. In some continental areas, short scale anisotropy, the result of a complex history, might be important and even might mask the large-scale anisotropy more related to present convective processes. This last statement settles on the following observation: when making a comparison with plate velocities directions, it is found a good statistical agreement between both directions (Fig. 7); this result shows that to first order, seismic anisotropy is reflecting the large scale plate tectonic motions. The differences between anisotropy and tectonic plate directions are related to more complex processes, as we will see below in the section *Oceanic Plates*.

ANISOTROPY IN THE DIFFERENT LAYERS OF THE EARTH AND THEIR GEODYNAMIC APPLICATIONS

Before considering measurements of anisotropy at global, regional or local scales, let us consider the laterally averaged Earth or equivalently, the spherically symmetric reference Earth models.

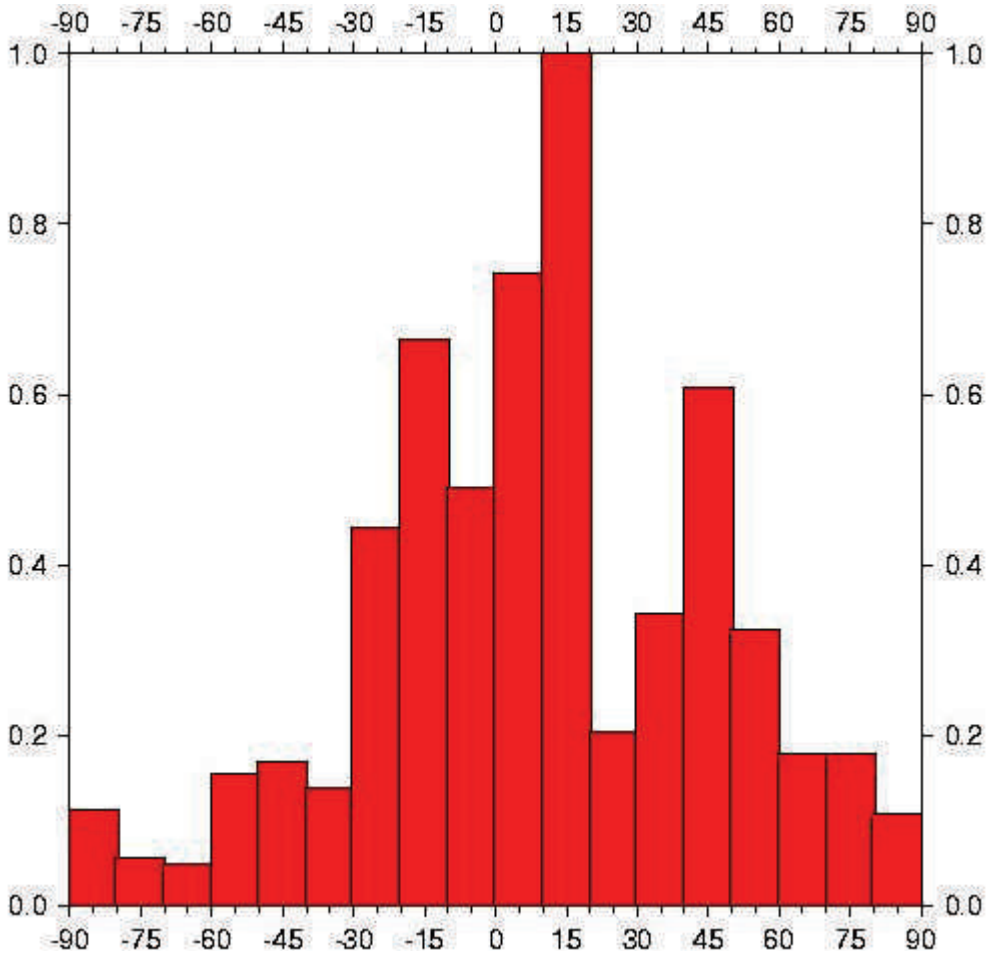

Figure 7. Histogram of the difference between plate velocities directions and synthetic SKS anisotropy azimuths in the Pacific plate.

Reference 1-D Earth models

Because tomographic models are derived from a reference model by linearized inversion schemes, there is a need for good starting radial reference models. The quality of the reference model will strongly condition the outcome of inversions for 3-D models. The most general case of anisotropy for a spherically symmetric earth is the transverse isotropy with vertical symmetry axis (also termed radial anisotropy). As discussed in the previous section, such a medium can be described using six functions of radius r, the density ρ, the wave velocities, V_{PH}, V_{SV}, and 3 anisotropic parameters ξ, ϕ and η readily related to A, C, F, L, N defined in the previous section.

PREM (Dziewonski and Anderson 1981) first introduced the radial anisotropy in the uppermost 220 km of the mantle. However, some aspects of the normal mode data are not well explained by PREM (Montagner and Anderson 1989a), for example fundamental toroidal mode and body wave travel times. There were several attempts to reconcile normal mode data and body wave data (Widmer 1991, Montagner and Kennett 1996).

Several robust features have been found regarding the radial anisotropy, from such inversions based on the different body-wave models [IASP91 (Kennett and Engdahl 1991); SP6 (Morelli and Dziewonski 1993); AK135 and AK303 (Kennett et al. 1996)]. First of all, anisotropy is significant in the whole upper mantle with a minimum value in the depth range 300-500 km. It is very small in the whole lower mantle except in a zone we call the “lower transition zone” (between the 660-km-discontinuity and 900-km depth)

and in the D″-layer. An interesting feature of these models is the existence of a complex radial anisotropy in the transition zone (410-660 km) and at the uppermost lower mantle (660-900 km), each zone presenting a different ξ $(= (V_{SH} / V_{SV})^2 - 1)$ -value pattern. The existence of anisotropy in the D″-layer seems robust as well, but is difficult to interpret, with a small S-wave anisotropy but large P-wave and η anisotropies. Therefore, these new reference Earth models provide some indication of the existence of anisotropy in three depth ranges, the first one in D″-layer at the core-mantle boundary, the second one around the 660-km-discontinuity. Independent seismological studies tend to corroborate these findings in the upper mantle, the transition zone, and the D″-layer.

Evidence of anisotropy in the upper 410 km of the mantle

The uppermost mantle down to 410 km is the range where the existence of seismic anisotropy is now widely recognized and well documented. Azimuthal variations have been found for body waves and surface waves in different areas of the world. During the last years, the shear wave splitting, primarily on SKS waves, was extensively used for studying continental deformation, but very few studies using body waves are devoted to oceanic areas. Conversely, global anisotropic tomographic models have been derived during the last 10 years from surface waves, but they are the most reliable below oceanic areas. Therefore the comparison of body wave and surface wave data is still in its infancy. However, as shown by Montagner et al. (2000) and Vinnik et al. (2002), such a comparison is providing encouraging results.

The seismic anisotropy in the Earth can therefore be retrieved by different methods from different datasets. We will only present some examples of interesting applications of anisotropy in large scale geodynamics and tectonics. The application of seismic anisotropy to geodynamics in the upper mantle is straightforward, if we assume that fast-polarization axis of mineralogical assemblages is in the flow plane parallel to the direction of flow (Fig. 1). Seismic anisotropy in the mantle is therefore reflecting the strain field prevailing in past (frozen-in anisotropy) for shallow layers or present convective processes in deeper layers. Therefore, it makes it possible to map convection in the mantle. It must be noted that, when only the radial anisotropy is retrieved, its interpretation is non-unique. A fine layering of the mantle can also generate such a kind of anisotropy, and neglecting the azimuthal anisotropy can bias the amplitude of radial anisotropy.

As mentioned in the previous section (Fig. 5), a complete interpretation of anisotropic tomography maps makes it necessary to simultaneously consider the maps of V_S, ξ and G parameters in order to separate the effects of temperature and orientation of flow. A discussion for the Earth can be found in Montagner and Guillot (2000). We will only focus on geodynamic consequences for oceanic plates and continents.

We will tentatively suppose that the direction of the flow in the mantle is directly related to the direction of azimuthal anisotropy or the sign of the radial anisotropy. This is approximately true in a rich-olivine mantle. A complete modeling of the relations between mantle flow and preferential orientations doesn't exist now, but this hypothesis seems quite reasonable, especially in regions where the strain field could have been quasi-stationary for millions of years.

Oceanic plates

Figure 8 shows 3 maps at depths of 100 km and 200 km displaying V_{SV} velocity anomalies (Fig. 8a) and the 2 kinds of anisotropy, which can be retrieved by simultaneous inversion of Rayleigh and Love waves constant 0-Ψ and azimuthal terms of Equation (5) from the model of Montagner (2002). On Figure 8b, the equivalent radial anisotropy of the medium, for S-wave expressed through the ξ parameter, is displayed. The maps of

Figure 8c are the distributions of the *G*-parameter related to the azimuthal variation of SV-wave velocity. The maximum amplitude of *G* is around 5% and is rapidly decreasing as depth is increasing. The distribution of anisotropy has completely different patterns and amplitudes at these 2 depths (100 and 200 km).

It shows that, to the first order, the agreement of directions of maximum velocity with plate tectonics is correct in the depth range 100 to 300 km (Montagner 1994). However, the azimuth of G-parameter can largely vary as a function of depth (Montagner and Tanimoto 1991). For instance, at shallow depths (down to 60 km), the maximum velocity can be parallel to mountain belts or plate boundaries (Vinnik et al. 1991, Silver 1996, Babuska et al. 1998), and orthogonal at large depth. This means that, at a given place, the orientation of fast axis is a function of depth, making difficult the interpretation of SKS splitting.

Since convective flow below oceans is dominated by large-scale plate motions, the long wavelength anisotropy found in oceanic lithospheric plates, should be similar to the smaller-scale anisotropy which should be measured from body waves. By the way, one of the first evidences of anisotropy was found in the Pacific Ocean by Hess (1964) for Pn-waves. Since that time, there were many measurements of the subcrustal anisotropy (see Babuska and Cara 1991, for a review). So far, there are very few measurements of anisotropy by SKS splitting in the oceans. Due to the lack of seismic stations on the seafloor (with the exception of H2O halfway between Hawaii and California), the only measurements available for SKS were performed in stations located on ocean islands (Ansel and Nataf 1989, Kuo and Forsyth 1992, Russo and Okal 1999, Wolfe and Silver 1998), which are by nature anomalous objects, such as volcanic hotspots where the strain field is perturbed by the ascending material and not necessarily representative of the main mantle flow field. SKS splitting was measured during the temporary MELT experiment on the East-Pacific Rise (Wolfe and Solomon 1998) but the orientation of the splitting is in disagreement with the predictions of Blackman et al. (1996). Walker et al. (2001) presented a first measurement of SKS splitting at H2O, but it is in disagreement with independent SKS splitting measurement at the same station by Vinnik et al. (2002) and with surface wave anisotropy (Montagner 2002).

There were other attempts of determining anisotropy for other kinds of body waves such as ScS and multiple ScS (Ando 1984, Farra and Vinnik 1994, Gaherty et al. 1995), or differential times of sS-S, or SS-S waves (Kuo et al. 1987, Sheehan and Solomon 1991, Fischer and Yang 1994, Gaherty et al. 1995, Fouch and Fischer 1996, Yang and Fischer 1994), however, only surface wave inversion can provide a 3-D map of anisotropy below oceans. Radial cross-sections show that the ξ parameter is usually negative and small (in any case smaller than average), where flow is primarily radial (mid-ocean ridges and subducting zones). Between plate boundaries, oceans display very large areas with a large positive radial anisotropy such as in the Pacific Ocean (Ekström and Dziewonski 1997), characteristic of an overall horizontal flow field. Oceanic plates are zones where the comparison between directions of plate velocities (Minster and Jordan 1978) or NUVEL-1 (DeMets et al. 1990) and directions of *G*-parameter is the most successful

Figure 8 (next page). Result of the simultaneous inversion of Rayleigh and Love waves dispersion and their azimuthal variations at 100 km depth (left) and 200 km depth (right). (adapted from Montagner 2002). (Top): Distribution of the V_{SV} parameter in %. (Middle): ξ distributions in % with respect to ACY400 (Montagner and Anderson 1989b). Be aware that ξ anomalies are plotted with respect to a reference value different from 0. (Bottom): Anisotropy map of the G-parameter (V_{SV} azimuthal anisotropy).

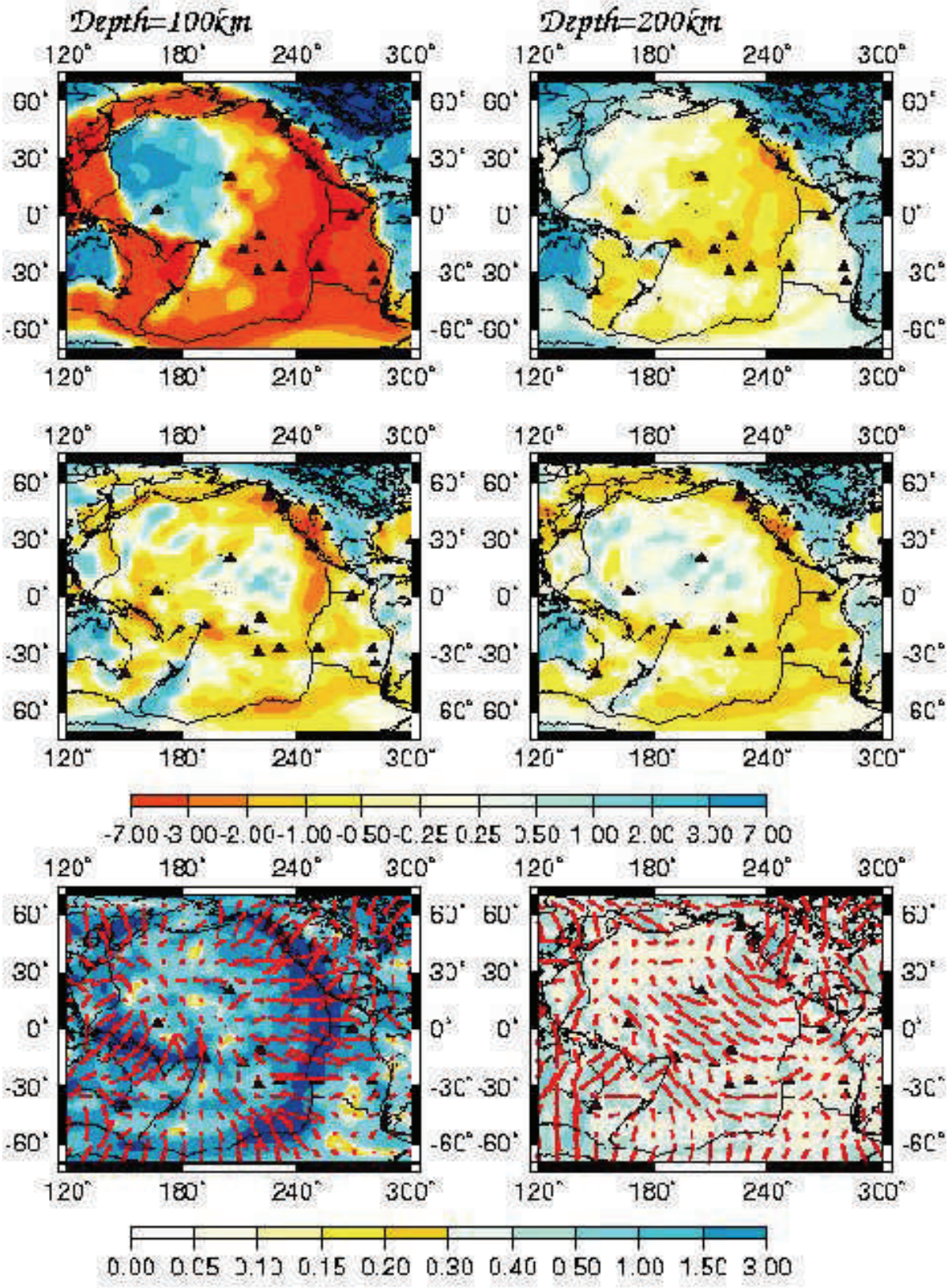
Depth=100km
Depth=200km
120° 180° 240° 300°
60° 30° 0° -30° -60°
-7.00 -3.00 -2.00 -1.00 -0.50 -0.25 0.25 0.50 1.00 2.00 3.00 7.00
0.00 0.05 0.10 0.15 0.20 0.30 0.40 0.50 1.00 1.50 3.00

in the asthenosphere down to 250-300 km (Montagner 1994). Conversely, such a comparison is more controversial below plates bearing a large proportion of continents, such as the European-Asian plate, characterized by a very small absolute motion in the hotspot coordinate system.

Oceans are the areas where Plate tectonics applies almost perfectly. The large-scale azimuthal anisotropy within and below lithosphere is closely related to plate motions (Montagner 1994) and modeled in this framework (Tommasi et al. 1996). The map of the *G*-parameter at 100 km shows that the azimuthal anisotropy is very large along spreading ridges with a large asymmetry for the East Pacific rise. The direction of anisotropy is in very good agreement with plate motion. The anisotropy is large as well in the middle of the Pacific plate, but it can be observed that there is a line of very small azimuthal anisotropy almost parallel to the EPR. This linear area of small anisotropy was coined Low Anisotropy Channel by Montagner (2002). They are presumably related to cracking within the Pacific plate and/or to secondary convection within and below the rigid lithosphere, predicted by numerical and analog experiments. These new features provide strong constraints on the decoupling between the plate and asthenosphere. The existence and location of these LACs might be related to the current active volcanoes and hotspots (possibly plumes) in Central Pacific. LACs, which are dividing the Pacific Plate into smaller units, might indicate a future reorganization of plates with ridge migrations in the Pacific Ocean. They call for more thorough numerical modelling.

Continents

Seismic anisotropy can provide fundamental information on the structure of continents, their root and the geodynamic processes involved in mountain building and collision between continents (Vinnik et al. 1992, Silver 1996) such as in Central Asia (Griot et al. 1998a,b). ξ is usually very heterogeneous below continents in the first 150-200 km of depth with positive or negative areas according to geology. But it seems to display a systematic tendency of being positive at larger depth (down to 300 km), whereas it is very large in the oceanic lithosphere in the depth range 50 to 200 km and decreases rapidly at larger depths (Montagner 1994). Conversely, radial anisotropy is displaying a maximum (though smaller than in oceanic lithosphere) below very old continents (such as Siberian and Canadian Shield) in the depth range 200 to 400 km. Seismic anisotropy below continents, sometimes confined to the upper 220 km (Gaherty and Jordan 1995) can still be significant below. A more quantitative comparison of radial anisotropy between different continental provinces is presented in Babuska et al. (1998), and demonstrates systematic differences according to the tectonic context. The existence of positive large-scale radial anisotropy below continents at depth might be a good indicator of the continental root which was largely debated since the presentation of the model of tectosphere by Jordan (1978, 1981). If we assume that this maximum of anisotropy is related to an intense strain field in this depth range, it might be characteristic of the boundary between continental lithosphere and "normal" upper mantle material. And our results show that the root of continents as defined by anisotropy is located between 200 and 300 km. Such a result was recently confirmed for the Australian continent by Debayle and Kennett (2000) and Simmons et al. (2002).

It must be emphasized that the anisotropy near the surface is probably different from the deep one. Part of the observed anisotropy might be related to the fossil strain field prevailing during the setting of materials and the deeper part is related to the present strain field. If we bear in mind that the anisotropy displayed from surface waves is the long wavelength filtered anisotropy (approximately 1500 km), it can be easily understood that the average anisotropy displayed from surface waves in the first 200 km might be very different from the one found from body waves. The tectonic structure of continents

is the result of a long and complex history. The characteristic length scale under continents is related to the size of blocks successively accreted to existing initial cores and probably smaller than 1500 km. This statement is supported by different studies of SKS body waves that demonstrate that the direction of maximum velocity can change on horizontal scales smaller than 100 km (Vinnik et al. 1991, Silver 1996). The fact that we do not observe a systematic behaviour in the first hundreds of kilometers for similar continental geological zones, does not mean that anisotropy is not present but only that its characteristic scale is different from one region to another one. Due to the low pass filtering effect of surface wave tomographic technique, the long wavelength signature of anisotropy is diluted.

The measurement of seismic anisotropy can provide fundamental information for the understanding of tectonic processes. Silver (1996) and Savage (1999) present reviews of the information provided by shear-wave splitting beneath continents. The poor lateral resolution of global scale anisotropic tomography can be considered as a strong limitation in continental areas. This technique can only be efficiently applied in areas where large-scale coherent processes are present. The best candidate where this condition is fulfilled in continents, is the collision zone between India and Asia, where the applicability of plate tectonics can be questioned.

Griot et al. (1998a) undertook such an investigation in Central Asia. The primary goal of this study was the discrimination between two competing extreme models of deformations, the heterogenous model of Avouac and Tapponnier (1993) and the homogeneous model of England and Houseman (1986). It was necessary to use shorter wavelength surface waves (40-200 s) in order to obtain a lateral resolution of 350 km. Synthetic models of seismic anisotropy can be inferred from the heterogeneous and homogeneous models. In order to perform correct and quantitative comparisons between observed seismic anisotropy and the deformation models, the short wavelengths of the synthetic models (spatial scale smaller than 350 km) were filtered out. The statistical comparison between observed and synthetic azimuthal anisotropies for both models enables to determine in different depth ranges, which deformation model dominates. Griot et al. (1998b) show that the heterogeneous model is in better agreement with observations in the first 200 km, whereas the homogeneous model better fits the deep anisotropy below 200 km. We must be aware that such a comparison is only valid from a statistical point of view and that a comparison at a more local scale (the scale of body wave measurements) might display some differences with the observed SKS anisotropy. This kind of investigation only underlines large scale ongoing and prevailing active processes and is not devoted to a precise measurement of anisotropy at any specific place. It demonstrates that in the uppermost 200 km, the tectonics is well described by the relative movement of continental blocks and that plate tectonics can apply to these plate-like areas.

Seismic anisotropy can now be used for making quantitative measurements. By using simultaneously splitting data and geodetic data, Silver and Holt (2002) were able to calculate the relative motion of lithospheric plate and asthenosphere. They show that the mantle trails the hotspot motion of the plate. This results show a weak coupling between lithosphere and asthenosphere, in contrast with the Pacific plate, where the coupling (reflected by plate direction) is the first-order effect in the uppermost 200 km, whereas LACs (Low Anisotropy channels) suggesting some decoupling, is a second-order effect.

The fossil shallow anisotropy (first 100 kilometers) that reflects the past strain field, should be very useful for understanding the processes involved in surficial tectonics (see review in Savage 1999). If we were able to determine the age of establishment of this shallow anisotropy, the measurement of this kind of anisotropy should open wide a new field in Earth sciences: the Paleo-Seismology which might provide fundamental

information to structural seology.

Anisotropy in the transition zone

The transition zone plays a key role in mantle dynamics, particularly the 660-km-discontinuity which might inhibit the passage of matter between the upper and the lower mantle. Its seismic investigation is made difficult on global scale by the poor sensitivity of fundamental surface waves in this depth range and by the fact that teleseismic body waves recorded at continental stations from earthquakes primarily occurring along plate boundaries have their turning point below the transition zone. However, Montagner and Kennett (1996), by using eigen-frequency data, display some evidence of radial anisotropy in the upper (410-660 km) and lower (660-900 km) transition zones. Another important feature of the Transition zone is that, contrarily to the rest of the upper mantle, the upper transition zone is characterized by a large degree 2 pattern (Masters et al. 1982), and to a less extent, the degree 6. Montagner and Romanowicz (1993) explained this degree 2 pattern by the predominance of a simple large-scale flow pattern characterized by two upwellings in central Pacific Ocean and Eastern Africa and two downwellings in the Western and Eastern Pacific Ocean. This scheme was corroborated by the existence in the upper transition zone of a slight but significant radial anisotropy displayed by Montagner and Tanimoto (1991) and Roult et al. (1990). In the Transition zone, the pattern of radial anisotropy is dominated by degree 4 in agreement with the prediction of this model. Therefore, the observations of the geographical distributions of degrees 2, 4, 6 in the transition zone are coherent and spatially dependent. Montagner (1994) compared these different degrees to the corresponding degrees of the hotspot and slab distribution. In this simple framework, the distribution of plumes and slabs are merely a consequence of the large-scale simple flow in the transition zone.

The existence of anisotropy close to the 660-km-discontinuity was also found by Vinnik and Montagner (1996) below Germany and Vinnik et al. (1998) in central Africa. By studying P-to-S converted waves at the GRF network and at GEOSCOPE station BNG in central Africa, they observed that part of the initial P-wave is converted into SH-wave. This signal can be observed on the transverse component of seismograms. The amplitude of this SH-wave cannot be explained by a dipping 660-km-discontinuity and it constitutes a good evidence for the existence of anisotropy just above this discontinuity. However, there is some evidence of lateral variation of anisotropy in the transition zone as found by the investigation of several subduction zones (Fischer and Yang 1994, Fischer and Wiens 1996). Fouch and Fischer (1996) present a synthesis of these different studies and show that some subduction zones such as Sakhalin Islands requires deep anisotropy in the transition zone, whereas others such as Tonga do not need any anisotropy. They conclude that their data might be reconciled by considering the upper transition zone (410-520 km) intermittently anisotropic, and the rest of the transition zone might be isotropic.

The evidence of anisotropy in the transition zone was confirmed recently by 2 independent studies, using different datasets. Wookey et al. (2002) present evidence of very large S-wave splitting (up to 7 s) in the vicinity of the 660-km-discontinuity between Tonga-Kermadec subduction zone and Australia. On a global scale, Trampert and van Heijst (2002) show a robust long-wavelength azimuthal anisotropic structure in the transition zone. The rms amplitude of lateral variations of G is about 1%. The interpretation of these new exciting results is not obvious but they confirm that the transition zone might be a mid-mantle boundary layer.

Anisotropy in the D″-layer

During the last years, the structure of the mysterious D″-layer has been extensively investigated. It is not the goal of this paper to review these different studies which make

use of different kinds of body waves but only to draw attention to recent results which make evident the presence of anisotropy in the D″-layer (Vinnik et al. 1989, Lay and Young 1991). The search for anisotropic structures in the D″-layer might provide fundamental information on boundary layer shear flow, partial melt or slab remnants at core-mantle boundary. There seems to be a general consensus that, except the D″-layer, the lower mantle does not contribute significantly to shear wave splitting observation. However, we must be aware that it might not be valid everywhere, and part of the anisotropy attributed to D″-layer might originate in the lowermost mantle. For example, differential splitting between phases such as $P_{660}S$ and SKS phases, or between SKS and SKKS, indicate that at least some regions of the lower mantle contain significant anisotropy (Iidaka and Niu 1998, Barruol and Hoffman 1999, Vinnik et al. 1997). Actually, the main drawback to investigate anisotropy in the lower mantle results from the limited crossing ray coverage. In addition, it is necessary to get rid of the influence of the anisotropy in the upper mantle. Therefore, it is not yet clear if lower mantle anisotropy is only localized in the bottom boundary layer (D″ layer) or if there are some areas within the lower mantle with significant anisotropy.

So far, there is clear evidence of anisotropy in the D″-layer. By studying Sd-waves (S diffracted waves at the Core-Mantle boundary), Vinnik et al. (1995) found that SVd-waves is delayed relative to SHd-waves by 3s. Their observations are characteristic of a transversely isotropic medium with vertical symmetry axis with $V_{SH} > V_{SV}$. Other seismic observations such as anomalous diffraction of body waves (Maupin 1994) confirm this kind of anisotropy and its rapid lateral variation is made evident in many areas around the world (see review in Lay et al. (1998)) such as in Caribbean Sea (Kendall and Silver 1996), North America (Matzel et al. 1996, Garnero and Lay 1996), Indian Ocean (Ritsema 2000). The origin of anisotropy observed in D″-layer is still debated (Kendall and Silver 1996, Kendall 2000) and might be due to horizontal layering in connection with paleo-subduction and/or aligned inclusions inducing different velocities for SV and SH (SPO anisotropy). On the same line, McNamara et al. (2001) showed that near cold downwellings, LPO may dominate, while near warm upwellings, SPO might be a more likely candidate. Numerical calculations of mantle convection (McNamara 2002) show that the slab deformation in the deep mantle, inducing large-strain deformation at high stresses can explain the presence of strong anisotropy in D″-layer.

NUMERICAL MODELING AND BOUNDARY LAYERS

In the previous section, we have highlighted the presence of seismic anisotropy in different parts of the Earth, using both body and surface wave data. This review of the presence of anisotropy in different layers of the Earth demonstrated that the anisotropy is a very general feature. However, it is not present in all depth ranges nor at all scales. As discussed in the first section, the observation of seismic anisotropy due to LPO at large scales requires several strong conditions, starting with the presence of anisotropic crystals up to the existence of an efficient large scale present or past strain field. Theoretical studies suggest that, when anisotropic minerals such as olivine are deformed, their crystallographic axes develop a systematic relationship to the principal axes of finite strain, and the amplitudes of the anisotropy is grossly proportional to the amplitude of the finite strain until it reaches a steady state (McKenzie 1979, Ribe 1989, Ribe and Yu 1991, Kaminski and Ribe 2001). Many numerical modelings of the convective mantle show that in a convective system, the strain field is not spatially uniform (Chastel et al. 1993). Streamlines are much more concentrated in boundary layers than in the middle of the cells. The consequence is that the amplitude of the strain field and of the seismic anisotropy resulting from the lattice preferred orientation (Tommasi et al. 2000), is very heterogeneous and the largest in boundary layers.

For filling the gap between grain scale modeling and large scale anisotropy measurements, there is now a real need for making more quantitative comparisons between seismic anisotropy and numerical modeling. Gaboret et al. (2002) calculated the convective circulation in the mantle by converting perturbations of S-wave velocity into density perturbations. Figure 9 shows 2 cross-sections through the Pacific hemisphere and the associated flow lines derived from the tomographic model of Ekstrom and Dziewonski (1998). This kind of modeling enables to calculate the strain tensor and to test different hypotheses for the prevailing mechanisms of alignment, by comparison with seismic data. We present in Figure 10 a first attempt to compare azimuthal anisotropy of the global anisotropic model of Montagner (2002) and the maximum horizontal stretching rate. The cosine of the difference between the fast axis of V_{SV} and the axis of horizontal extensional rate, is plotted. The best agreement is found for young ages in the Pacific ocean. More generally, the comparison is correct for oceanic plates but not so good for continental plates, where the resulting anisotropy displays a more complex distribution.

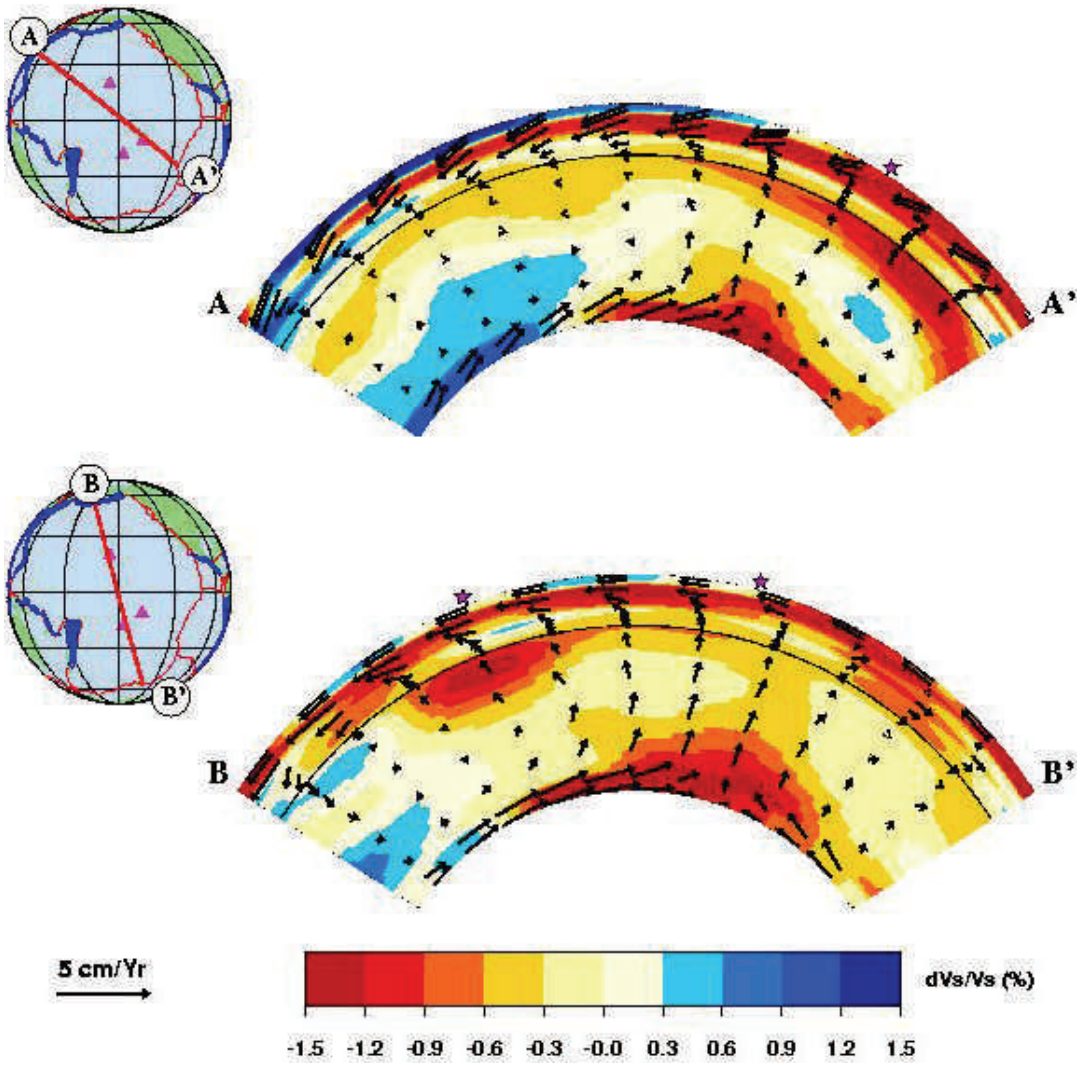

Figure 9. Two whole mantle cross-sections through the Ekstrom and Dziewonski tomographic model (1998) along great circles. Also shown in the inset maps are triangles which represent the locations of 3 Pacific hotspots. The superimposed black arrows in the cross-sections represent the mantle flow velocities predicted on the basis of the buoyancy forces derived from shear velocity anomalies. (adapted from Gaboret et al. 2002).

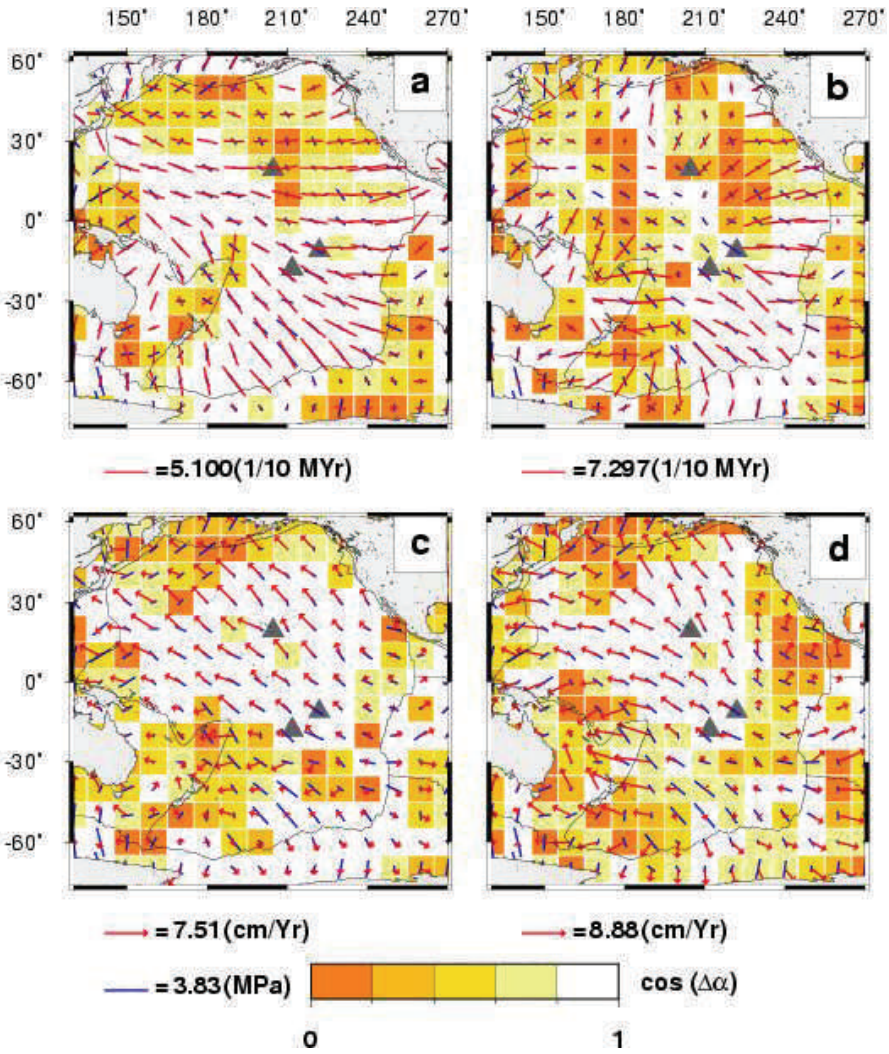

Figure 10. Comparison of azimuthal seismic anisotropy and the direction of maximum stretching predicted by the flow model presented in Figure 9. [(Adapted from Gaboret et al. (2002).]

Conversely, we can assume that the observation of mantle seismic anisotropy is the indication of a strong present-day strain field (at the exception of crust, topmost oceanic, and continental lithosphere where fossil anisotropy may be present). This strain field can be associated with boundary layers. In the previous sections, we saw that there are good evidences of the presence of seismic anisotropy in the D″-layer, in the transition zone and in the uppermost mantle. These findings are summarized in Figure 11.

The D″-layer and the uppermost mantle have been related to boundary layers of the mantle convective system for a long time. The D″-layer above the core-mantle boundary is characterized by a large degree of seismic heterogeneities and anisotropy with V_{SH} larger than V_{SV}. It might be at the same time, the graveyard of subducted slabs and the source of megaplumes. D″- anisotropy can be related either to horizontal layering (lattice- and shape- preferred orientations) of cold material or the presence of aligned inclusions owing to the presence of melt (Kendall and Silver 1996, McNamara et al. 2002). For the uppermost oceanic mantle, seismic anisotropy is present in both lithosphere and asthenosphere, and for oceans, some finite-element models are able to quantitatively relate lithospheric and asthenospheric strain to anisotropy (Tommasi et al. 1996). But the

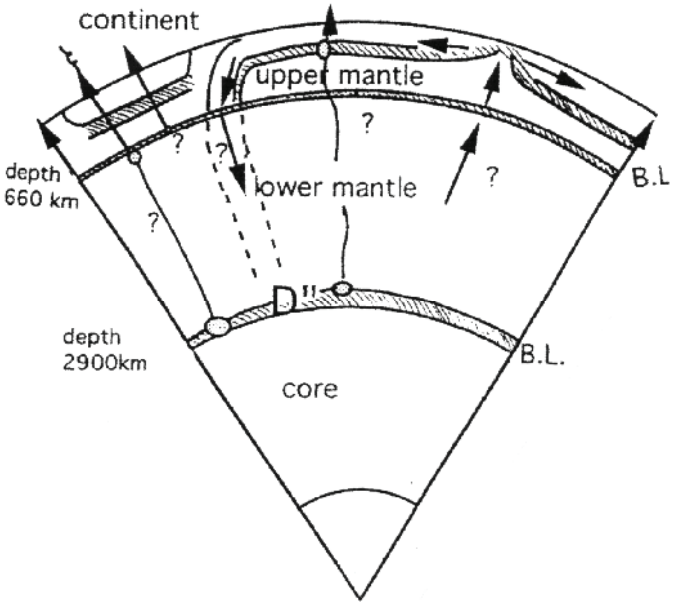

Figure 11. Cross-section of the Earth from the core-mantle boundary up to the surface. The hatched (respectively dotted) areas show where there are robust evidence of present (resp. fossil) anisotropy. B.L. stands for Boundary Layer.

presence of anisotropy in the transition zone (Montagner and Kennett 1996, Vinnik and Montagner 1996, Wookey et al. 2002, Trampert and van Heijst 2002) is fundamental and problematic, because it provides a new clue that the transition zone could act as a secondary boundary layer. The first evidence of anisotropy in the transition zone tends to favor the predominance of horizontal flow over vertical flow. The major consequence of this finding is that the transition zone (down to about 900-1000 km) is dividing, on average, the mantle into two convective systems, the upper mantle and the lower mantle. This general statement does not rule out the possibility that flow circulation between the upper and the lower mantle is occuring. But, it means that the exchange of matter between the upper and the lower mantle is difficult. It is too early to assess the amount of matter going through, from measurements of seismic anisotropy, but the complete mapping of seismic anisotropy in the transition zone (Trampert and van Heijst 2002) associated with numerical modeling might enable to put constraints on the flow between the upper and lower mantles.

CONCLUSIONS : FROM SEISMIC ANISOTROPY TO ANISOTROPIC SEISMOLOGY

We have presented in this paper different observations of seismic anisotropy and their applications in geology and geodynamics. Seismic anisotropy is able to define continental roots, to investigate the coupling between different layers, to discriminate different geodynamic processes and competing convective models. Three boundary layers were so far detected by seismic anisotropy: the uppermost mantle, the transition zone (though new work is necessary to understand its role) and the D″-layer. Other applications of seismic anisotropy can be easily found. For example, Montagner and Anderson (1989a) show that the different anisotropic parameters might be used for discriminating competing petrological models such as pyrolite or piclogite. Some seismologists claim that the temporal variation of anisotropy in the crust might be an efficient tool for investigating and monitoring the earthquake cycle (Crampin and Booth 1985, Crampin and Volti 1999). The temporal changes in shear-wave polarization were successfully used to show the variation of the stress regime before and after a volcanic eruption (Miller and Savage 2001). Seismic anisotropy starts to be used in seismic exploration for monitoring oil reservoirs. Therefore, to study time-dependent phenomena, seismic anisotropy turns out to be very efficient. The scientific potential of seismic

anisotropy is enormous and largely unexploited. In conclusion, the seismic anisotropy provides a new dimension in the investigation of processes of our dynamic Earth.

ACKNOWLEDGMENTS

We are grateful to Don Anderson, Adam Dziewonski, Andrea Morelli, Lev Vinnik, Mike Gurnis, Jeroen Ritsema, Jeroen Tromp, Barbara Romanowicz, Anne Davaille, Alessandro Forte, Goran Ekström, for fruitful discussions.

This is I.P.G.P. contribution # 1878.

APPENDIX A. BASIC THEORY OF WAVE PROPAGATION IN ANISOTROPIC MEDIA

In any elastic medium, and in neglecting all additional terms due to prestress, gravity, inertial terms, the equation of motion is:

$$\rho \frac{\partial^2 u_i}{\partial_t^{\,2}} = \frac{\partial}{\partial x_j} \sigma_{ij}$$

where ρ is the density, u_i the components of the displacement, σ_{ij} the components of the stress tensor. There is a linear relationship between the stress tensor and the strain tensor

$$\varepsilon_{kl} = \frac{1}{2}\left(u_{k,l} + u_{l,k}\right),$$

such that:

$$\sigma_{ij} = C_{ijkl}\, \varepsilon_{kl}$$

Let us consider ω the angular frequency of the wave, and $\boldsymbol{k}$ its propagation vector, while $\boldsymbol{\nu} = \boldsymbol{k}/k$ is a unit vector in the direction of $\boldsymbol{k}$. The equations of motion simplify to:

$$\rho\, \omega^2\, u_i = k_j\, k_k\, C_{ijkl}\, u_l$$

We look for a solution on the form of a plane wave:

$$u_i = a_i \exp\left(i\omega \left(t - \frac{\nu_q x_q}{V} \right) \right)$$

where V is the phase velocity, a_i the components of the polarization vector $\boldsymbol{a}$, ν_k the unit vector of the wave vector $\boldsymbol{\nu}$. For a wave propagating in direction $\boldsymbol{e_1}$:

$$\rho V^2 a_1 = C_{1111}\, a_1 + C_{1112}\, a_2 + C_{1113}\, a_3$$
$$\rho V^2 a_2 = C_{2111}\, a_1 + C_{2112}\, a_2 + C_{2113}\, a_3$$
$$\rho V^2 a_3 = C_{3111}\, a_1 + C_{3112}\, a_2 + C_{3113}\, a_3$$

These three equations can be written in a condensed way:

$$(\, \boldsymbol{T} - \rho\, V^2\, \boldsymbol{I}\,)\, \boldsymbol{a} \;=\; 0$$

where

$$T = \begin{pmatrix} C_{1111} & C_{1112} & C_{1113} \\ C_{2111} & C_{2112} & C_{2113} \\ C_{3111} & C_{3112} & C_{3113} \end{pmatrix}$$

is the Christoffel matrix, ***I*** the identity matrix. That is an eigenvalue problem which has 3 real positive roots for ρV^2 with orthogonal eigenvectors. Therefore, these equations demonstrate that there are 3 body waves in every direction of phase propagation with orthogonal particle motion and with velocities which in general are different and vary with direction. In case of isotropic medium the elastic tensor is invariant with rotation, and T is a diagonal matrix:

$$T = \begin{pmatrix} \lambda + 2\mu & 0 & 0 \\ 0 & \mu & 0 \\ 0 & 0 & \mu \end{pmatrix}$$

The well-known isotropic velocities can be written immediately:

$$V = V_P = \sqrt{\frac{\lambda + 2\mu}{\rho}} \quad , \quad \text{and} \quad V_P = \sqrt{\frac{\mu}{\rho}} \quad \text{(repeated root).}$$

In case of weak anisotropy, we can define quasi P-waves and quasi S-waves, but in case of very strong anisotropy, the eigenvectors can have any orientation which can be very different from quasi P- and quasi S-waves. An important consequence is that the propagation of energy of a plane wave is no longer in the direction of the propagation vector.

APPENDIX B. TENSORS AND MATRICES MANIPULATIONS

The effect of intrinsic anisotropy has been extensively studied in laboratory and in the field. Most crystals present in the Earth are strongly anisotropic (olivine, pyroxenes) except garnet.

A medium is perfectly elastic when a linear relationship (Hooke's law) relates the stress tensor σ_{ij} and the strain tensor ε_{kl}. A general elastic medium is anisotropic since its physical properties are dependent on its geometrical orientation. The anisotropic properties of any elastic medium are usually described by its fourth-order elastic tensor C_{ijkl} which linearly relates the stress tensor $\boldsymbol{\sigma}$ and the strain tensor $\boldsymbol{\varepsilon}$, as seen in the previous section.

Contraction of indices. Instead of keeping 4 indices, it is common, for sake of simplicity to write the elastic tensor C_{ijkl} as a matrix (6 × 6) by using the following rules (the reader must be aware that for avoiding mathematical errors, it is easier to perform calculations by using the fourth-order elastic tensor C_{ijkl}):

c_{ijkl} C_{pq}

(3×3×3×3) (6×6)

$p = i=j$ *if* $i = j$; $q = k = l$ *if* $k = l$

$p = 9\text{-}i\text{-}j$ *if* $i \neq j$; $q = 9\text{-}k\text{-}l$ *if* $k \neq l$

This is the Voigt notation. It allows to obtain simplified matrix representations for elastic tensors:

- Isotropic elastic tensor (2 independent parameters):

$$\begin{pmatrix} \lambda+2\mu & \lambda & \lambda & 0 & 0 & 0 \\ 0 & \lambda+2\mu & \lambda & 0 & 0 & 0 \\ 0 & 0 & \lambda+2\mu & 0 & 0 & 0 \\ 0 & 0 & 0 & \mu & 0 & 0 \\ 0 & 0 & 0 & 0 & \mu & 0 \\ 0 & 0 & 0 & 0 & 0 & \mu \end{pmatrix}$$

- Elastic tensor of a transversely isotropic medium with a vertical symmetry axis (5 independent parameters):

$$\begin{pmatrix} A & A-2N & F & 0 & 0 & 0 \\ A-2N & A & F & 0 & 0 & 0 \\ F & F & C & 0 & 0 & 0 \\ 0 & 0 & 0 & L & 0 & 0 \\ 0 & 0 & 0 & 0 & L & 0 \\ 0 & 0 & 0 & 0 & 0 & N \end{pmatrix}$$

- Elastic tensor of a general orthorhombic medium with three mutually perpendicular symmetry planes (9 independent parameters):

$$\begin{pmatrix} a & b & c & 0 & 0 & 0 \\ b & d & e & 0 & 0 & 0 \\ c & e & f & 0 & 0 & 0 \\ 0 & 0 & 0 & g & 0 & 0 \\ 0 & 0 & 0 & 0 & h & 0 \\ 0 & 0 & 0 & 0 & 0 & i \end{pmatrix}$$

These expressions are valid, for a given symmetry, only in a specific co-ordinate system, the crystal reference frame, where the reference axes are simply related to the symmetry elements of the medium (see Nye 1957, e.g.). In the general case, the components of the tensor are expressed in another reference frame, which can be related to the crystal reference frame by a 3-D rotation. This rotation is a linear transformation of the basis vectors of the crystal reference frame, and as any linear transformation it can be represented by a matrix $\boldsymbol{A}$, whose components are written $A_i{}^j$. The components C'_{mnpq} of the fourth-order elastic tensor in the new reference frame, after rotation, are related to the crystal frame components C_{ijkl} as:

$$C'_{mnpq} = A^i_m \, A^j_n \, A^k_p \, A^l_q \, C_{ijkl}$$

Note that this expression is only valid for the covariant components of the elastic tensor, in the general case. For the contravariant and mixed components, e.g., see Hladik (1995). In this paper, the elastic tensor is expressed in the usual 3-D (real) Cartesian reference frame, $\boldsymbol{A}$ represents a rotation and is then an orthogonal real matrix, so the expression above is valid for all types of components.

Elastic matrix: scale of aggregates. For polycrystals, problems of averaging arise. There are different ways to make averages. Let n_m be the number of different crystalline

populations, and α_q their proportion in the aggregate. Each mineral of a given population has its elasticity described by the elastic tensor *C,* with components C_{ijkl}^{q}. These quantities are called stiffnesses. We also introduce the compliance tensor *S*, whose components S_{ijkl} are defined by: $\varepsilon_{ij} = S_{ijkl}\,\sigma_{kl}$.

Different averages among the most commonly used are (Watt et al. 1976):

- Voigt average: hypothesis of constant deformation. We obtain for the stiffnesses:

$$C_{ijkl}^{V} = \sum_{q=1}^{nm} \alpha_q C_{ijkl}^{q}$$

- Reuss average: hypothesis of constant stress. We obtain for the compliances:

$$S_{ijkl}^{V} = \sum_{q=1}^{nm} \alpha_q S_{ijkl}^{q}$$

After some manipulations (matrix inversion in the most general case), the associated stiffnesses C_{ijkl}^{R} can be calculated (Nye 1957).

- Voigt-Reuss-Hill average: it is only the arithmetic mean of the Voigt and Reuss averages, and has no theoretical justification.

- Hashin-Shtrikman: Minimization of the elastic energy (no analytical solution in the most general case).

A more thorough description of these averages as well as others can be found in Mainprice et al. (2000).

REFERENCES

Aki K, Kaminuma K (1963) Phase velocity of Love waves in Japan (part 1): Love waves from the Aleutian shock of March 1957. Bull Earthquake Res Inst 41:243-259

Anderson DL (1961) Elastic wave propagation in layered anisotropic media. J Geophys Res 66:2953-2963

Anderson DL (1989) Theory of the Earth. Blackwell Scientific Publications, Oxford, UK

Anderson DL, Bass JD (1984) Mineralogy and composition of the upper mantle. Geophys Res Lett 1: 637-640

Anderson DL, Bass JD (1986) Transition region of the Earth's upper mantle. Nature 320:321-328

Anderson DL, Regan J (1983) Upper mantle anisotropy and the oceanic lithosphere. Geophys Res Lett 10:841-844

Ando M (1984) ScS polarization anisotropy around the Pacific Ocean. J Phys Earth 32:179-196

Ando M, Ishikawa Y, Yamazaki F (1983) Shear wave polarization anisotropy in the upper mantle beneath Honshu, Japan. J Geophys Res 88:5850-5864

Ansel V, Nataf HC (1989) Anisotropy beneath 9 stations of the Geoscope broadband network as deduced from shear wave splitting. Geophys Res Lett 16:409-412

Avouac JP, Tapponnier P (1993) Kinematic model of active deformation in central Asia. Geophys Res Lett 20:895-898

Babuska V, Cara M (1991) Seismic Anisotropy in the Earth. Kluwer Academic Press, Dordrecht, The Netherlands

Babuska V, Montagner JP, Plomerova J, Girardin N (1998) Age-dependent large-scale fabric of the mantle lithosphere as derived from surface-wave velocity anisotropy. Pure Appl Geophys 151:257-280

Backus GE (1962) Long wave elastic anisotropy produced by horizontal layering. J Geophys Res 67: 4427- 4440

Backus GE (1965) Possible forms of seismic anisotropy of the upper mantle under oceans. J Geophys Res 70:3249-3439

Barruol G, Hoffman R (1999) Upper mantle anisotropy beneath the GEOSCOPE stations. J Geophys Res 104:10757-10774

Blackman DK, Kendall JM, Dawson PR, Wenk HR, Boyce D, Morgan JP (1996) Teleseismic imaging of subaxial flow at mid-ocean ridges: Travel-time effects of anisotropic mineral texture in the mantle. Geophys J Intl 127:415-426

Bostock MG (1997) Anisotropic upper-mantle stratigraphy and architecture of the Slave craton. Nature 390:392-395
Bowman JR, Ando M (1987) Shear-wave splitting in the upper mantle wedge above the Tonga subduction zone. Geophys J R Astron Soc 88:25-41
Cara M, Leveque JJ (1988) Anisotropy of the asthenosphere: The higher mode data of the Pacific revisited. Geophys Res Lett 15:205-208
Chastel YB, Dawson PR, Wenk HR, Bennett K (1993) Anisotropic convection with implications for the upper mantle. J Geophys Res 98:17757-17771
Christensen NI, Lundquist S (1982) Pyroxene orientation within the upper mantle. Bull Geol Soc Am 93:279-288
Crampin S (1984) An introduction to wave propagation in anisotropic media. Geophys J R Astron Soc 76:17-28
Crampin S, Booth DC (1985) Shear-wave polarizations near the North Anatolian fault, II: Interpretation in terms of crack-induced anisotropy. Geophys J R Astron Soc 83:75-92
Crampin S, Volti T, Stefansson R (1999) A successfully stress-forecast earthquake. Geophys J Intl 138: F1-F5
Debayle E (1999) SV-wave azimuthal anisotropy in the Australian upper mantle: preliminary results from automated Rayleigh waveform inversion. Geophys J Intl 137:747-754
Debayle E, Lévêque JJ (1997) Upper mantle heterogeneities in the Indian Ocean from waveform inversion. Geophys Res Lett 24:245-248
Debayle E, Kennett BLN (2000) Anisotropy in the Australasian upper mantle from Love and Rayleigh waveform inversion. Earth Planet Sci Lett 184:339-351
Dziewonski AM, Anderson DL (1981) Preliminary Reference Earth Model. Phys Earth Planet Inter 25: 297-356
Ekström G, Dziewonski AM (1998) The unique anisotropy of the Pacific upper mantle. Nature 394:168-172
England P, Houseman G (1986) Finite strain calculations of continental deformation, 2. Comparison with the India-Asia collision zone. J Geophys Res 91:3664-3676
Estey LH, Douglas BJ (1986) Upper mantle anisotropy: A preliminary model. J Geophys Res 91:11393-11406
Farra V, Vinnik LP (1994) Shear-wave splitting in the mantle of the Pacific. Geophys J Intl 119:195-218
Fedorov F (1968) Theory of Elastic waves in crystals. Plenum Press, New York
Fischer KM, Wiens DA (1996) The depth distribution of mantle anisotropy beneath the Tonga subduction zone. Earth Planet Sci Lett 142:253-260
Fischer KM, Yang X (1994) Anisotropy in Kuril-Kamtchatka subduction zone structure. Geophys Res Lett 21:5-8
Forsyth DW (1975) The early structural evolution and anisotropy of the oceanic upper mantle. Geophys J R Astron Soc 43:103-162
Forsyth DW, Webb SC, Dorman LM, Shen Y (1998) Phase velocities of Rayleigh waves in MELT experiment on the East Pacific Rise. Science 280:1235-1238
Fouch MJ, Fischer KM (1996) Mantle anisotropy beneath northwest Pacific subduction zones. J Geophys Res 101:15987-16002
Fouch MJ, Fischer KM, Parmentier EM, Wysession ME, Clarke TJ (2000) Shear wave splitting, continental keels, patterns of mantle flow. J Geophys Res 105:6255-6275
Fouch MJ, Fischer KM, Wysession ME (2001) Lowermost mantle anisotropy beneath the Pacific: Imaging the source of the Hawaiian plume. Earth Planet Sci Lett 190:167-180
Fukao Y (1984) Evidence from core- reflected shear waves for anisotropy in the Earth's mantle. Nature 309:695-698
Gaboret C, Forte A, Montagner JP (2002) The unique dynamics of the Pacific hemisphere mantle and its signature on seismic anisotropy. Earth Planet Sci Lett (submitted)
Gaherty JB, Jordan TH (1995) Lehmann discontinuity as the base of the anisotropic layer beneath continents. Science 268:1468-1471
Garnero EJ, Lay T (1996) Lateral variation in lowermost mantle shear wave anisotropy beneath the North Pacific and Alaska. J Geophys Res 102:8121-8135
Griot DA, Montagner JP, Tapponnier P (1998a) Surface wave phase velocity and azimuthal anisotropy in Central Asia. J Geophys Res 103:21215-21232
Griot DA, Montagner JP, Tapponnier P (1998b) Heterogeneous versus homogeneous strain in Central Asia. Geophys Res Lett 25:1447-1450
Hadiouche O, Jobert N, Montagner JP (1989) Anisotropy of the African continent inferred from surface waves. Phys Earth Planet Inter 58:61-81
Hager B, O'Connell R (1979) Kinematic models of large-scale flow in the Earth's mantle. J Geophys Res 84:1031-1048

Helbig K (1994) Foundations of Anisotropy for Exploration Seismics. Pergamon/Elsevier Science, Oxford, UK
Hess H (1964) Seismic anisotropy of the uppermost mantle under the oceans. Nature 203:629-631
Hladik J (1995) Le calcul tensoriel en physique. Paris, Masson, France.
Hirn A, Jiang M, Sapin M, Diaz J, Nercessian A, Lu QT, Lépine JC, Shi DN, Sachpazi M, Pandy MR, Ma K, Gallart J (1995) Seismic anisotropy as an indicator of mantle flow beneath the Himalayas and Tibet. Nature 375:571-574
Iidaka T, Niu F (1998) Evidence for an anisotropic lower mantle beneath eastern Asia: comparison of shear wave splitting data of SKS and P660s. Geophys Res Lett 25:675-678
Jordan TH (1978) Composition and development of the continental tectosphere. Nature 274:544-548
Jordan TH (1981) Continents as a chemical boundary layer. Phil Trans R Soc London Ser A 301:359-373
Jung HY, Karato SI (2001) Water-induced fabric transitions in olivine. Science 293:1460-1462
Kaminski E, Ribe NM (2001) A kinematic model for recrystallization and texture development in olivine polycrystals. Earth Planet Sci Lett 189:253-267
Karato S-i (1989) Seismic anisotropy: mechanisms and tectonic implications. *In* Rheology of Solids and of the Earth. S-i Karato, M Toriumi (eds) Oxford University Press, Oxford, p 393-42
Karato SI, Li P (1993) Diffusive creep in perovskite: Implications for the rheology of the lower mantle. Science 255:771-778
Kendall JM (2000) Seismic anisotropy in the boundary layers of the mantle. *In* Earth's Deep Interior: Mineral physics and tomography from the atomic to the global scale. Karato S-i, Forte A, Liebermann RC, Masters G, Stixrude L (eds) Am Geophys Union Monograph, Washington, DC
Kendall JM, Silver PG (1996) Constraints from seismic anisotropy on the nature of the lowermost mantle. Nature 381:409-412
Kennett BLN, Engdahl ER (1991) Traveltimes for global earthquake location and phase identification. Geophys J Intl 105:429-465
Larson EWF, Tromp J, Ekstrom G (1998) Effects of slight anisotropy on surface waves. Geophys J Intl 132:654-666
Laske G, Masters G (1998) Surface-wave polarization data and global anisotropic structure. Geophys J Intl 132:508-520
Lavé J, Avouac JP, Lacassin R, Tapponnier P, Montagner JP (1996) Seismic anisotropy beneath Tibet: Evidence for eastward extrusion of the Tibetan lithosphere? J Geophys Res 140:83-96
Lay T, Williams Q, Garnero EJ, Kellog L, Wysession ME (1998) Seismic wave anisotropy in the D" region and its implications. *In* Core-Mantle Boundary Region. Gurnis M, Wysession ME, Knittle E, Buffett B (eds) Geodynamic Series 28:229-318
Lévêque JJ, Cara M (1985) Inversion of multimode surface wave data: evidence for sub--lithospheric anisotropy. Geophys J R Astron Soc 83:753-773
Lévêque JJ, Cara M, Rouland D (1991) Waveform inversion of surface-wave data: a new tool for systematic investigation of upper mantle structures. Geophys J Intl 104:565-581
Levshin A, Ratnikova L (1984) Apparent anisotropy in inhomogeneous media. Geophys J R Astron Soc 76: 65-69
Love AEH (1927) A Treatise on the Theory of Elasticity, 4th Edition. Cambridge University Press, Cambridge, UK
Mainprice DG, Barruol G, Ben Ismail W (2000) The seismic anisotropy of the Earth's. mantle: From single crystal to Polycrystal. *In* Earth's Deep Interior: Mineral Physics and Tomography From the Atomic Scale to the Global Scale. Geophys Monogr 117:237-264
Masters G, Jordan TH, Silver PG, Gilbert F (1982) Aspherical Earth structure from fundamental spheroidal-mode data. Nature 298:609-613
Matzel E, Sen MK, Grand SP (1996) Evidence for anisotropy in the deep mantle beneath Alaska. Geophys Res Lett 23:2417-2420
Maupin V (1994) On the possibility of anisotropy in the D" layer as inferred from the polarization of diffracted S-waves. Phys Earth Planet Inter 87:1-32
McEvilly TV (1964) Central U.S. crust-upper mantle structure from Love and Rayleigh wave phase velocity inversion. Bull Seism Soc Am 54:1997-2015
McKenzie D (1979) Finite deformation during fluid flow. Geophys J R Astron Soc 58:687-715
McNamara AK, Karato SI, van Keken PE (2001) Localization of dislocation creep in the lower mantle; implications for the origin of seismic anisotropy. Earth Planet Sci Lett 191:85-99
McNamara AK, van Keken PE, Karato SI (2002) Development of anisotropic structure in the Earth's lower mantle by solid-state convection. Nature 416:310-314
Meade C, Silver PG, Kaneshima S (1995) Laboratory and seismological observations of lower mantle anisotropy. Geophys Res Lett 22:1293-1296
Miller V, Savage S (2001) Changes in seismic anisotropy after volcanic eruptions: Evidence from Mount Ruapehu. Science 293:2231-2233

Minster JB, Jordan TH (1978) Present-day plate motions. J Geophys Res 83:5331-5354
Mitchell BJ, Yu GK (1980) Surface wave dispersion, regionalized velocity models and anisotropy of the Pacific crust and upper mantle. Geophys J R Astron Soc 63:497-514
Mochizuki E (1986) The free oscillations of an anisotropic and heterogeneous Earth. Geophys J R Astron Soc 86:167-176
Montagner JP (1985) Seismic anisotropy of the Pacific Ocean inferred from long-period surface wave dispersion. Phys Earth Planet Inter 38:28-50
Montagner JP (1986a) First results on the three dimensional structure of the Indian Ocean inferred from long period surface waves. Geophys Res Lett 13:315-318
Montagner JP (1986b) Regional three-dimensional structures using long-period surface waves. Ann Geophys 4:B3:283-294
Montagner JP (1994) What can seismology tell us about mantle convection? Rev Geophys 32:2:115-137
Montagner JP (1998) Where can seismic anisotopy be detected in the Earth's mantle? In boundary layers. Pure Appl Geophys 151:223-256
Montagner JP (2002) Upper mantle low anisotropy channels below the Pacific Plate. Earth Planet Sci Lett (in press)
Montagner JP, Anderson DL (1989a) Constraints on elastic combinations inferred from petrological models. Phys Earth Planet Inter 54:82-105
Montagner JP, Anderson DL (1989b) Constrained reference mantle model. Phys Earth Planet Inter 58: 205-227
Montagner JP, Griot DA, Lavé J (2000) How to relate body wave and surface wave anisotropies? J Geophys Res 105:19015-19027
Montagner JP, Guillot L (2000) Seismic anisotropy tomography. *In* Problems in Geophysics for the Next Millennium. E Boschi, G Ekström, A Morelli (eds) Editrice Compositori, Bologna, Italy, p 217-254
Montagner JP, Jobert N (1988) Vectorial Tomography. II: Application to the Indian Ocean. Geophys J R Astron Soc 94:309-344
Montagner JP, Kennett BLN (1996) How to reconcile body-wave and normal-mode reference Earth models? Geophys J Intl 125:229-248
Montagner JP, Lognonné P, Beauduin R, Roult G, Karczewski JF, Stutzmann E (1998) Towards multiscale and multiparameter networks for the next century: The French efforts. Phys Earth Planet Inter 108: 155-174
Montagner JP, Nataf HC (1986) On the inversion of the azimuthal anisotropy of surface waves. J Geophys Res 91:511-520
Montagner JP, Nataf HC (1988) Vectorial Tomography. I: Theory. Geophys J R Astron Soc 94:295-307
Montagner JP, Tanimoto T (1990) Global anisotropy in the upper mantle inferred from the regionalization of phase velocities. J Geophys Res 95:4797-4819
Montagner JP, Tanimoto T (1991) Global upper mantle tomography of seismic velocities and anisotropies. J Geophys Res 96:20337-20351
Montagner JP, Romanowicz B, Karczewski JF (1994) A first step towards an Oceanic Geophysical Observatory. EOS, Trans Am Geophys Union 75:150-154
Montagner JP, Romanowicz B (1993) Degrees 2, 4, 6 inferred from seismic tomography. Geophys Res Lett 20:631-634
Morelli A, Dziewonski AM, Woodhouse JH (1986) Anisotropy of the inner core inferred PKIKP travel times. Geophys Res Lett 13:1545-1548
Morelli A, Dziewonski AM (1993) Body wave traveltimes and a spherically symmetric P- and S-wave velocity model. Geophys J Intl 112:178-194
Nataf HC, Nakanishi I, Anderson DL (1984) Anisotropy and shear velocity heterogeneities in the upper mantle. Geophys Res Lett 11:109-112
Nataf HC, Nakanishi I, Anderson DL (1986) Measurement of mantle wave velocities and inversion for lateral heterogeneity and anisotropy, III. Inversion. J Geophys Res 91:7261-7307
Nicolas A (1993) Why fast polarization directions of SKS seismic waves are parallel to mountain belts? Phys Earth Planet Inter 78:337-342
Nicolas A, Boudier F, Boullier AM (1973) Mechanisms of flow in naturally and experimentally deformed peridototes. Am J Sci 273:853-876
Nicolas A, Christensen NI (1987) Formation of anisotropy in upper mantle peridotites: A review. *In* Composition, Structure and Dynamics of the Lithosphere/Asthenosphere System. Fuchs K, Froidevaux C (eds) American Geophysical Union, Washington, DC, p 111-123
Nishimura CE, Forsyth DW (1989) The anisotropic structure of the upper mantle in the Pacific. Geophys J 96:203-229
Nye JF (1985) Physical Properties of Crystals: Their Representation by Tensors and Matrices. Reprint (with corrections). Clarendon Press, Oxford, UK
Park J, Levin V (2002) Seismic anisotropy: tracing plate dynamics in the mantle. Science 296:485-489

Peselnick L, Nicolas A, Stevenson PR (1974) Velocity anisotropy in a mantle peridotite from Ivrea zone: Application to uper mantle anisotropy. J Geophys Res 79:1175-1182
Peselnick L, Nicolas A (1978) Seismic anisotropy in an ophiolite peridotite: Application to oceanic upper mantle. J Geophys Res 83:1227-1235
Pettersen O, Maupin V (2002) Lithospheric anisotropy on the Kerguelen hotspot track inferred from Rayleigh wave polarisation anomalies. Geophys J Intl 149:225-246
Ribe NM (1989) Seismic anisotropy and mantle flow. J Geophys Res 94:4213-4223
Ribe NM, Yu Y (1991) A theory for plastic deformation and textural evolution of olivine polycrystals. J Geophys Res 96:8325-8335
Ricard Y, Nataf HC, Montagner JP (1996) The 3S-Mac model: confrontation with seismic data. J Geophys Res 101:8457-8472
Ringwood AE (1975) Composition and Petrology of the Earth's Mantle. McGraw-Hill, New York, 618 p
Ritsema J (2000) Evidence for shear wave anisotropy in the lowermost mantle beneath the Indian Ocean. Geophys Res Lett 27:1041-1044
Roult G, Rouland D, Montagner JP (1994) Antarctica II: Upper mantle structure from velocity and anisotropy. Phys Earth Planet Inter 84:33-57
Rümpker G, Silver PG (1998) Apparent shear-wave splitting in the presence of vertically varying anisotropy. Geophys J Intl 135:790-800
Russo R, Silver PG (1994) Trench-parallel flow beneath the Nazca plate from seismic anisotropy. Science 263:1105-1111
Russo RM, Okal EA (1999) Shear wave splitting and upper mantle deformation in French Polynesia: Evidence for small-scale heterogeneity related to the Society hotspot. J Geophys Res 103:15089-15107
Savage MK (1999) Seismic anisotropy and mantle deformation: What have we learned from shear wave splitting? Rev Geophys 37:65-106
Schlue JW, Knopoff L (1977) Shear--wave polarization anisotropy in the Pacific Ocean. Geophys J R Astron Soc 49:145-165
Silver PG (1996) Seismic anisotropy beneath the continents: Probing the depths of geology. Ann Rev Earth Planet Sci 24:385-432
Silver PG, Chan WW (1988) Implications for continental structure and evolution from seismic anisotropy. Nature 335:34-39
Silver PG, Chan WW (1991) Shear wave splitting and subcontinental mantle deformation. J Geophys Res 96:16429-16454
Silver PG, Holt WE (2002) The mantle flow field beneath North America. Science 295:1054-1057
Silveira G, Stutzmann E, Montagner JP (1998) Mendes-Victor L. Anisotropic tomography of the Atlantic Ocean from Rayleigh surface waves. Phys Earth Planet Inter 106:259-275
Simmons FJ, van der Hilst R, Montagner JP, Zielhuis A (2002) Multimode Rayleigh wave inversion for shear wave speed heterogeneity and azimuthal anisotropy of the Australian upper mantle. Geophys J Intl (in press)
Singh S, Taylor M, Montagner JP (2002) On the presence of liquid in Earth's inner core. Science 287: 2471-2474
Smith ML, Dahlen FA (1973) The azimuthal dependence of Love and Rayleigh wave propagation in a slightly anisotropic medium. J Geophys Res 78:3321-3333
Smith ML, Dahlen FA (1975) Correction to 'The azimuthal dependence of Love and Rayleigh wave propagation in a slightly anisotropic medium'. J Geophys Res 80:1923
Suetsugu D, Nakanishi I (1987) Regional and azimuthal dependence of phase velocities of mantle Rayleigh waves in the Pacific Ocean. Phys Earth Planet Inter 47:230-245
Tanimoto T (1986) Free oscillations in a slightly anisotropic Earth. Geophys J R Astron Soc 87:493-517
Tanimoto T, Anderson DL (1985) Lateral heterogeneity and azimuthal anisotropy of the upper mantle: Love and Rayleigh waves 100-250s. J Geophys Res 90:1842-1858
Tommasi A, Mainprice D, Canova G, Chastel Y (2000) Viscoplastic sel-consistent and equilibrium-based modeling of oilivine preferred orientations: Implications for the upper mantle anisotropy. J Geophys Res 105:7893-7908
Tommasi A, Vauchez A, Russo R (1996) Seismic anisotropy in ocean basins: Resistive drag of the sublithospheric mantle? Geophys Res Lett 23:2991-2994
Trampert J, Woodhouse JH (1996) Global phase velocity maps of Love and Rayleigh waves between 40 and 150 seconds. Geophys J Intl 212:675-690
Trampert J, van Heijst HJ (2002) Global anisotropy azimythal anisotropy in the transition zone. Science 296:1297-1299
van der Hilst RD, Karason H (1999) Compositional heterogeneity in the bottom 1000 km of the Earth's mantle: Toward a hybrid convection model. Science 283:1885-1888
Vauchez A, Nicolas A (1991) Mountain building: strike-parallel motion and mantle anisotropy. Tectonophysics 185:183-191

Vinnik LP, Chevrot S, Montagner JP (1998) Seismic evidence of flow at the base of the upper mantle. Geophys Res Lett 25:1995-1998

Vinnik LP, Farra V, Romanowicz B (1989b) Azimuthal anisotropy in the earth from observations of SKS at GEOSCOPE and NARS broadband stations. Bull Seism Soc Am 79:1542-1558

Vinnik LP, Kosarev GL, Makeyeva LI (1984) Anisotropiya litosfery po nablyudeniyam voln SKS and SKKS. Dokl Akad Nauk USSR 278:1335-1339

Vinnik LP, Kind R, Kosarev GL, Makeyeva LI (1989a) Azimuthal Anisotropy in the lithosphere from observations of long-period S-waves. Geophys J Intl 99:549-559

Vinnik LP, Makayeva LI, Milev A, Usenko AY (1992) Global patterns of azimuthal anisotropy and deformations in the continental mantle. Geophys J Intl 111:433-447

Vinnik LP, Montagner JP (1996) Shear wave splitting in the mantle from Ps phases. Geophys Res Lett 23:2449-2452

Vinnik LP, Romanowicz B, Le Stunff Y, Makayeva L (1995) Seismic anisotropy in D"-layer. Geophys Res Lett 22:1657-1660

Vinnik LP, Montagner JP, Girardin N, Dricker I (2002) Saul, Shear wave splitting at H2O: A comment. Geophys Res Lett (submitted)

Walker KT, Bokelmann GH, Klemperer SL (2001) Shear-wave splitting to test mantle Deformation models around Hawaii. Geophys Res Lett 28:4319-4322

Watt JP, Davies GF, O'Connell (1976) The elastic properties of composite materials. Rev Geophys Space Phys 14:541-565

Widmer R, Masters G, Gilbert F (1993) Spherically symmetric attenuation within the Earth from normal mode data. Geoph J Intl 104:541-553

Wolfe JW, Silver PG (1998) Seismic anisotropy of oceanic upper mantle: Shear wave splitting methodologies and observations. J Geophys Res 103:749-771

Woodhouse JH, Giardini D, Li XD (1986) Evidence for inner core anisotropy from free oscillations. Geophys Res Lett 13:1549-1552

Wookey J, Kendall JM, Barruol G (2002) Mid-mantle deformation inferred from seismic anisotropy. Nature 415:777-780

Yu Y, Park J (1993) Anisotropy and coupled long-period surface waves. Geophys J Intl 114:473-489

Zhang S, Karato S-i (1995) Lattice preferred orientation of olivines aggregates deformed in simple shear. Nature 375:774-777